UNIVERSIDADE ESTADUAL DE CAMPINAS
INSTITUTO DE QUÍMICA

CARLOS MARROTE MANZANO

Transition metal complexes with ibuprofen hydrazide: synthesis, characterization and biological assays.

Complexos de metais de transição com hidrazida do ibuprofeno: síntese, caracterização e ensaios biológicos.

Campinas
2018

CARLOS MARROTE MANZANO

Transition metal complexes with ibuprofen hydrazide: synthesis, characterization and biological assays.

Complexos de metais de transição com hidrazida do ibuprofeno: síntese, caracterização e ensaios biológicos.

Masters dissertation presented to the institute of Chemistry of the University of Campinas as part of the requirements to obtain the title of Master in Chemistry, in the area of Inorganic Chemistry.

Dissertação de mestrado apresentada ao Instituto de Química da Universidade Estadual de Campinas como parte dos requisitos exigidos para obtenção do título de Mestre em Química na área de Química Inorgânica.

Orientador: Prof. Dr. Pedro Paulo Corbi

THIS COPY CORRESPONDS TO THE FINAL VERSION OF THE MASTER'S DISSERTATION DEFENDED BY CARLOS MARROTE MANZANO AND SUPERVISED BY PROF. DR. PEDRO PAULO CORBI

ESTE EXEMPLAR CORRESPONDE À VERSÃO FINAL DA DISSERTAÇÃO DEFENDIDA PELO ALUNO CARLOS MARROTE MANZANO, E ORIENTADA PELO PROF. DR. PEDRO PAULO CORBI.

Campinas

2018

Agência(s) de fomento e nº(s) de processo(s): CNPq, 130967/2016-5
ORCID: https://orcid.org/0000-0002-0969-223X

Ficha catalográfica
Universidade Estadual de Campinas
Biblioteca do Instituto de Química
Camila Barleta Fullin - CRB 8462

M319t

Manzano, Carlos Marrote, 1993-
Transition metal complexes with ibuprofen hydrazide : synthesis, characterization and biological assays / Carlos Marrote Manzano. – Campinas, SP : [s.n.], 2018.

Orientador: Pedro Paulo Corbi.
Dissertação (mestrado) – Universidade Estadual de Campinas, Instituto de Química.

1. Platina. 2. Paládio. 3. Compostos antitumorais. 4. Agentes antibacterianos. I. Corbi, Pedro Paulo. II. Universidade Estadual de Campinas. Instituto de Química. III. Título.

Informações para Biblioteca Digital

Título em outro idioma: Complexos de metais de transição com hidrazida do ibuprofeno : síntese, caracterização e ensaios biológicos
Palavras-chave em inglês:
Platinum
Palladium
Antitumoral compounds
Antibacterial agents
Área de concentração: Química Inorgânica
Titulação: Mestre em Química na área de Química Inorgânica
Banca examinadora:
Pedro Paulo Corbi [Orientador]
Ítalo Odone Mazali
Wilton Rogério Lustri
Data de defesa: 21-02-2018
Programa de Pós-Graduação: Química

BANCA EXAMINADORA

Prof. Dr. Pedro Paulo Corbi (Orientador)

Prof. Dr. Wilton Rogério Lustri (Universidade de Araraquara – UNIARA)

Prof. Dr. Italo Odone Mazali (IQ – UNICAMP)

A Ata de defesa com as respectivas assinaturas dos membros encontra-se no processo de vida acadêmica do aluno.

Este exemplar corresponde à redação final da Dissertação de Mestrado defendida pelo aluno **CARLOS MARROTE MANZANO**, aprovada pela Comissão Julgadora em 21 de fevereiro de 2018.

Acknowledgments

I would like to thank my family (Antonio, Vera, Fabio and Cesar), all my friends from LQBM (Douglas, Julia, Raphael, Anna Karla, Ana Thereza, Paula, Pedro, Laís and Mariana) and from the neighbor laboratories (Caio, Stephanie, Rennan, Bruno, Vera, Pamyla, Kalil, Naheed, Luís, Marcio, Marcos Ribeiro, Marcos Antonio, Adriana, Augusto, Lucas, Prof. Juliano, Prof. Diego and Prof. André) for the support and attention during these years. Also, I cannot thank enough my supervisor Prof. Pedro Corbi for all the help and the friendship that we built since I joined the group years ago. In addition to all of these incredible people, I am particularly grateful to my partner in science and in life, Mariana Ciol, who shared all the good and bad moments by my side.

Special thanks to: Dr. Fernando R. G. Bergamini for the aid during the project, especially with the DTF calculations; Prof. Dr. André L. B. Formiga from Inorganic Chemistry department – UNICAMP, for the insights concerning the DFT calculations and crystal structure; Prof. Dr. Wilton Rogério Lustri from Biological and Health Sciences Department, University of Araraquara - UNIARA for the antibacterial assays; Prof. Dra. Ana Lúcia T. G. Ruiz from the Faculty of Pharmaceutical Sciences (FCF) and Chemical, Biological and Agricultural Pluridisciplinary Research Center (CPQBA) – UNICAMP for the antiproliferative assays and Prof. Dr. Marcos A. Ribeiro for the refinement of the crystal structure.

I want to highlight and appreciate the importance of the lab technicians that were essential for this work, such as Cintia, Diego and Acacia from our lab, Gustavo and Anderson from NMR labs, Claudia and Sonia from spectroscopic labs, Deborah from single crystal X-ray analysis, Raquel, Fabi, and many others.

This study was supported by grants from Brazilian Agencies FAPESP (São Paulo State Research Council, grants #2015/25114-4 and #2013/22127-2), CAPES (Coordination for the Improvement of Higher Level Personnel) and CNPq (National Council for Scientific and Technological Development, grant #442123/2014-0). I am also grateful to CENAPAD-SP for computational facilities in which all DFT calculations were performed.

Resumo

Devido a importância de complexos metálicos na medicina, como cisplatina (e seus derivados), sulfadiazina de prata e auranofina, novos compostos de coordenação tem sido estudados como potenciais candidatos a fármacos para aplicação na clínica médica.

O desenvolvimento de um câncer pode estar intimamente ligado a processos inflamatórios. Existem estudos que sugerem que a ingestão regular de ibuprofeno e outros anti-inflamatórios não esteroidais protege contra o surgimento e crescimento de diversos tipos de câncer. Além disso, muitas moléculas que contém a função hidrazida tem mostrado um amplo espectro farmacológico, incluindo atividades antimicrobianas e antitumorais. Hidrazidas também são capazes de interagir com proteínas carreadoras que melhoram o perfil toxicológico e a seletividade frente a células tumorais.

Complexos de paládio(II) e platina(II) com uma hidrazida derivada do ibuprofeno (HIB) foram sintetizados e caracterizados por um conjunto de análises químicas e espectroscópicas. Os resultados das análises elementar e térmica, bem como dos estudos por espectrometria de massas (ESI-QTOF-MS), confirmaram as composições na razão 1:2:2 metal/HIB/cloreto. A estrutura cristalina do complexo de paládio(II) foi determinada por difratometria de raios X de monocristal. Este complexo apresenta a fórmula mínima $[PdCl_2(HIB)_2]$ com o ligante HIB coordenado ao íon metálico pelo grupo amina. Cálculos por DFT (Density Functional Theory) foram aplicados para que fosse possível sugerir a estrutura do complexo de Pt(II). As análises por ressonância magnética nuclear e espectroscopia no infravermelho reforçam que a coordenação observada na estrutura cristalina e calculada por DFT estão corretas. Ensaios de atividade antiproliferativa frente a células tumorais e não-tumorais e ensaios de inibição bacteriana foram realizados para avaliar a atividade biológica dos complexos obtidos. O complexo de Pd(II) mostrou-se ativo para a linhagem de câncer de ovário OVCAR-03 com boa seletividade. O complexo de Pt(II) não se mostrou ativo. Nenhum dos complexos foi ativo sobre as cepas bacterianas testadas. Também foram aplicadas técnicas de fluorescência e dicroísmo circular para avaliar a interação dos compostos com DNA, sendo que o complexo de Pd(II) foi o único capaz de interagir com DNA. Estes resultados sugerem que o DNA é um alvo biológico para o complexo de Pd(II).

Abstract

Given the importance of metal-based drugs such as cisplatin (and their derivatives), silver sulfadiazine and auranofin, novel metal complexes have been studied as promising drug candidates and are attracting attention in modern clinical medicine.

Cancer developing can be closely related to inflammatory processes. There are studies suggesting that the regular intake of ibuprofen and other non-steroidal anti-inflammatory drugs protect against the development of several types of cancer. Also, many molecules containing the hydrazide moiety have shown to have broad pharmacological activities, including antimicrobial and antitumor ones. These kind of compounds are known to interact with carrier proteins to improve their antitumor selectivity and toxicity profile and can also act as DNA modifying agents.

Palladium(II) and platinum(II) complexes with a hydrazide derivative of ibuprofen (HIB), were synthesized and characterized chemically and spectroscopically Elemental and TGA/DTA analyses as well as ESI-QTOF-MS analysis for both complexes confirmed a 1:2:2 metal/HIB/Cl^- ratio. The crystal structure of the palladium(II) complex was obtained and refined by single-crystal X-ray diffractometry, presenting a minimal formula of $[PdCl_2(HIB)_2]$ with HIB coordinating to the metal ion by the amine moiety. Density Functional Theory (DFT) calculations were also performed to propose the structure of the Pt(II) complex. Nuclear magnetic resonance and infrared spectroscopies reinforces the coordination observed in the crystal structure and DFT calculations. Antiproliferative and antibacterial assays *in vitro* were performed to evaluate the activity of the complexes obtained. The Pd(II) complex was active *in vitro* against the OVCAR-03 ovarian cancer cell line, with good selectivity. The Pt(II) complex showed no biological activity. Fluorescence and circular dichroism spectroscopic techniques were used to evaluate the interaction of the compounds with DNA. Only the Pd(II) complex was able to interact with this biomolecule, which suggests that DNA is a target for this compound.

Figures list

Tables list

Abbreviations list

CD…….....	Circular dichroism spectroscopy
CFU……..	Colony-forming unit
CSD…….……	Cambridge Structural Database
CT-DNA……..	Calf thymus - Deoxyribonucleic acid
DFT…….	Density Functional Theory
DMSO……..	Dimethyl sulfoxide
ESI-QTOF-MS.....	Electrospray ionization time of flight mass spectrometry
HIB…….……..	Ibuprofen hydrazide
HMBC…….……	Heteronuclear multiple bond coherence
HSQC……..…….	Heteronuclear single quantum coherence
ibu……..….....	Ibuprofen
IR…….....|	Infrared spectroscopy
MeOD……...	Methanol-d_3
MIC……..……	Minimal inhibitory concentration
NMR…….……	Nuclear magnetic resonance
HaCat …….....	Immortal keratinocyte (non-tumor human cell line).
NSAIDs…….....	Non-steroidal anti-inflammatory drugs
[$PdCl_2(HIB)_2$] or PdHIB…….....	Pd(II) complex with ibuprofen hydrazide
[$PtCl_2(HIB)_2$] or PtHIB……	Pt(II) complex with ibuprofen hydrazide
SSNMR...……	Solid state nuclear magnetic resonance
SYBR Green or SG……	Nucleic acid electrophoresis stain SYBR® Green I: N',N'-dimethyl-N-[4-[(E)-(3-methyl-1,3-benzothiazol-2-ylidene)methyl]-1-phenylquinolin-1-ium-2-yl]-N-propylpropane-1,3-diamine
TG/DTA……..	Thermogravimetric and differential thermal analysis
Tumor human cell lines……	U251 (glioma); UACC-62 (melanoma); MCF-7 (breast); NCI-ADR/RES (multidrug resistant ovarian); NCI-H460 (lung, non-small cells); PC-3 (prostate); OVCAR-03 (ovarian); HT-29 (colon); K562 (leukemia).

Summary

1. Introduction

1.1 The role of metal based drugs on cancer treatment

Cancer is one of the most significant public health case of concern in the world. According to the latest cancer report by the World Health Organization (WHO), cancer was responsible for 8.8 million deaths in 2015, which corresponds to nearly 1 in 6 deaths worldwide ["Cancer Fact sheet " World Health Organization, February 2017. Retrieved 24 August 2017].

Cancer can be defined as a collection of diseases related with abnormal and uncontrollable cell replication that may occur in any tissue. More specifically, cancer cells have self-sufficiency in growth signals and are insensitive to anti-growth signals, being capable to avoid mechanisms of apoptosis (programmable cell death), therefore they have unlimited replicative potential. Another important characteristic of cancer is the capacity to spread and invade different tissues, known as metastasis. This process is facilitated by sustained angiogenesis in the cancerous tissues[1].

Even though a great effort has been made over the past decades to treat cancer more effectively and safely, the pace of drug development is far behind the increasing rate of cancer incidence and mortality[2,3], mainly due to cancer heterogeneity and acquired resistance to conventional chemotherapeutic drugs[4]. Prospects by the U.S. National Cancer Institute show that the number of cancer cases will rise 50% and cancer deaths are projected to increase by 60% until 2030 ["The Burden of Cancer Worldwide" National Cancer Institute, Retrieved 24 August 2017]

The new era of metal-based drugs started in 1960´s when Barnett Rosenberg *et al.* showed the cisplatin capacity to inhibit cellular division in *Escherichia coli* [5]. This discovery lead to further studies in eukaryotic cells about its antitumor activity, and cisplatin became one of the most used and potent drugs against different types of cancer, such as lung, head and neck, testis and ovarian cancers. Nowadays, novel metal-based drugs are attracting attention in modern clinical medicine[6,7].

It is estimated that platinum drugs are used in 50% of all cancer chemotherapy[8], showing great results especially for testicular and ovarian cancer. However, limitations of their uses remain as a challenge to the scientific community. The increasing cisplatin cross-resistance developed by tumors, the narrow spectrum of antitumor activity, high toxicity and

challenging delivery are examples of these limitations[9,10]. In this context, in order to overcome the resistance in tumors, high systemic doses of the platinum-based drugs are necessary to achieve an effective intracellular concentration resulting in severe systemic toxicity[11].

Many derivatives of cisplatin were developed hoping to overcome part of such limitations. Figure 1 shows the platinum based drugs approved for use in medicine[12], in which cisplatin, carboplatin and oxaliplatin are approved worldwide, while nedaplatin, nobaplatin and heptaplatin are only approved to be used in Japan, China and Korea, respectively.

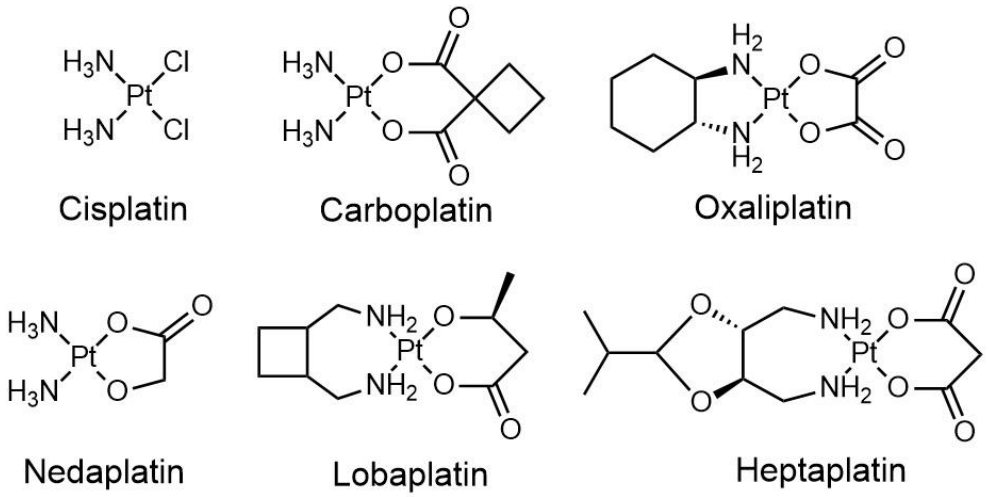

Figure 1. Platinum based drugs currently used in medical clinic.

The similarities between these drugs are promptly observed. All of them are Pt(II) complexes, with square geometries and ligands in a *cis* configuration. Pt(II) complexes act as prodrugs, requiring replacement of their labile ligands with water before they are able to bind and disrupt DNA function.[12] Generally, the toxicity of these drugs is directly related to the rate of exchange of the leaving groups for water molecules. For instance, cisplatin has two very labile chloride ligands that are easily substituted by water molecules in biological environments. Therefore it is significantly more toxic than the other Pt-based drugs that have bis-carboxylate ligands designed to increase the drug stability[13,14]. Other improvement made over the cisplatin structure is the addition of diamine bulky ligands ((1R,2R)-cyclohexane-1,2-diamine in the case of oxaliplatin) to overcome cisplatin cross-resistance by preventing binding of DNA repair proteins to Pt-DNA adducts[15].

Not only cis-Pt(II) drugs are known to have antitumor activity. Many trans-Pt(II) complexes were reported to be as active as cisplatin in various assays. Some of them have shown to be effective against cisplatin resistant cancer cells with slightly different

mechanisms.[16] Also, polynuclear platinum anti-cancer agents that have unique mechanisms of action were extensively studied by Farrell et. al. [17–19] and have great potential as new antitumor drugs.

Considering the successful application of platinum(II) complexes in cancer therapy and the similarity between platinum(II) and palladium(II) compounds, the latter metal was also considered in the synthesis of promising anticancer drugs, with good anticancer and antimicrobial *in vitro* and *in vivo* activities.[20] In general, Pd(II) coordination compounds have faster ligand exchange kinetics than their Pt(II) analogs, which usually causes rapid hydrolysis in biological medium, leading to higher toxicity and less systemic distribution.[21] For these reasons, its usually necessary to choose chelating ligands that stabilize the Pd(II) complexes, so that they reach the pharmacologic target. Palladium(II) complex are also usually more soluble than the correspondent Pt(II) complexes. [7,21]

There are different strategies that can be applied in the synthesis of new metal-based drugs for treatment of diseases as cancer. One of them is to align the cytotoxic properties of a metal ion with the desired activity of a specific ligand. An interesting approach is to use a particularly non-anticancer drug as ligand with favorable safety profile, known pharmacokinetics, coordination ability in the viewpoint of coordination chemistry and adequate permeability [2]. This approach was applied in the present work by choosing as ligand a derivative of ibuprofen in the synthesis of platinum(II) and palladium(II) complexes aiming the obtainment of new anticancer agents.

1.2 Ibuprofen: biological activities and applications in medicine

Ibuprofen is one of the most used non-steroidal anti-inflammatory drug (NSAID) in the medical clinic. It is used for the treatment of headache, muscular ache, arthritis rheumatoid, fever and pain related to tissue inflammation. Concerning cancer therapy, there are studies suggesting that the regular intake of ibuprofen and other NSAIDs protects against the development of many types of cancer including colon, breast, lung, and prostate cancer [22–24]. Cancer risk reductions are apparent after five or more years of regular anti-inflammatory use, with ibuprofen being the NSAID that produced the greater risk reductions (72% for colon cancer, 52% for breast cancer, 52% for lung cancer and 53% for prostate cancer)[22].

For ibuprofen, this property might be related to the chiral inversion pathway that converts the R-ibuprofen to its more effective anti-inflammatory enantiomer S-ibuprofen by the enzyme α-methylacyl-CoA racemase (AMACR). The organism processing of ibuprofen

reduces the normal activity of AMACR, which could reduce cancer developing. Although this mechanism study is still not conclusive, it is an interesting subject of study because AMACR is used as a marker (P504S) for several types of cancers[25,26].

Even though the role of ibuprofen appears to be in cancer prophylaxis rather than treatment, its interaction with a marker for cancer (AMACR – P504S)[27,28] by itself could be explored, using ibuprofen as an organic directing molecule and taking advantage of its pharmacological properties.

Concerning treatment and prevention of post-surgical infections, NSAIDs are commonly used concomitantly to antibiotics to reduce the level of tissue inflammation[29]. Therefore, anti-inflammatory ligands are particularly interesting for association with metal ions in the design and development of new pharmacological agents.

Given the relevance of ibuprofen, there are many examples of metal complexes with ibuprofen bearing antibacterial activity, such as silver(I) and gold(I) ibuprofen complexes[30,31] which are active against Gram-positive and Gram-negative strains and Pt(II) ibuprofen complex [Pt(1,2-diaminciclohexane)(ibuprofen)$_2$], which is active against Gram-positive microorganisms[32]. There is also a patent describing the use of Cu(II) and Zn(II) complexes with ibuprofen[33,34] as prophylaxis agents against cardiovascular inflammation and for prophylaxis and treatment of diabetes[30]. It is interesting to notice that none of these complexes were evaluated as antitumor agents, although complexes Au(I), Pt(II) and Cu(II) are usually evaluated as potential anticancer drugs[35].

Many derivatives of ibuprofen have been studied as well. Derivatives with s-triazines and 1,3-diaryl pyrazole, showed, respectively, higher analgesic and anti-inflammatory activities than free ibuprofen[36,37]. Moreover, ibuprofen conjugated with oligo(3-hydroxybutyrate) were able to inhibit *in vitro* proliferation of colon cancer cells (HT-29 and HCT 116)[38].

1.3 Hydrazides

Hydrazides and their derivatives are shown to have a broad pharmacological activities, including the antimicrobial and antitumor ones. For hydrazides and hydrazones of NSAIDs, the modification of the acidic site of these molecules are desired to partly reduce the adverse effects to the gastrointestinal tract[39,40].

There are several examples of biological active hydrazides[41]. Some of them are isonicotinohydrazide as an antituberculosis drug[42], N'-isopropylisonicotinohydrazide with antidepressant activity[43] and sulfonyl hydrazide derivatives that not only exhibit a wide range

of bacteriostatic activity, but also can act as DNA modifying agents. They have exhibited antitumor activities against murine tumors, including the B16 melanoma, M109 lung carcinoma, L1210 leukemia, P388 and M5076 reticulum cell sarcoma[44].

Regarding coordination chemistry, the derivatization of ibuprofen to a hydrazide adds two nitrogen atoms to the structure (see Figure 2) and introduces a new coordination site by the NH_2 group, in detriment of an acidic COOH coordination site. According to Pearson's acid base theory, stronger coordination bonds are formed by a pair of soft acid with soft base or hard acid with hard base[45]. Although classified as a hard base, nitrogen can be considered a softer Pearsons' bases than oxygen, being able to form more stable complexes with soft acids such as Pt(II) and Pd(II). As earlier discussed, the stability of Pt(II) and Pd(II) complexes, especially in biological environments, is desirable in most cases.

So, in this work we present the synthesis and characterization of new Pd(II) and Pt(II) complexes with a hydrazide derived from the NSAID ibuprofen (Figure 2) and the studies of the antiproliferative profile of the compounds over a panel of tumor cells and their activities over bacterial strains. Studies about interaction of the compounds with calf thymus DNA (CT-DNA) by circular dichroism and fluorescence spectroscopy were also performed to provide preliminary information about the mechanism of action of the complexes.

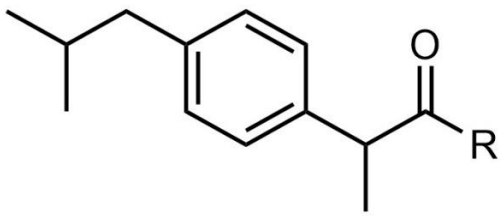

Figure 2. Ibuprofen (R = OH) and ibuprofen hydrazide (R = $NHNH_2$) molecular structures.

2. Objectives

2.1. General aims and scope

The aim of this work was synthesize an hydrazide of ibuprofen and its new metal complexes of Pt(II) and Pd(II), and evaluate their antitumor and antibacterial activities.

2.2. Specific objectives

- Optimize the synthesis of the ligand (ibuprofen hydrazide) and of the Pt(II) and Pd(II) complexes.
- Characterize the ligand and the corresponding complexes using chemical and spectroscopic techniques to determine their composition and structures.
- Use density functional theory (DFT) calculations to propose structures correlating with the experimental data.
- Evaluate the *in vitro* biological activity of the compounds against bacteria and cancer cells. Compare the activities observed for ligand and complexes.
- Study the interaction of the compounds with DNA and correlate the results with the biological activities.

3. Experimental section

3.1. Materials and Methods

Ibuprofen (racemic) was obtained from Maxpharm Industries. DNA sodium salt from calf-thymus type I, SYBR Green I 10,000x in DMSO and K_2PtCl_4 were purchased from Sigma–Aldrich Laboratories. K_2PdCl_4 and hydrazine hydrate (64%) were purchased from Acros Laboratories. Methyl chloroformate (99%), dichloromethane (99%) and triethylamine (99%) were purchased from Spectrum Chemical Mfg, LabSynth and Merck Laboratories, respectively. Triethylamine was purified by distillation with potassium carbonate while dichloromethane was purified by distillation with phosphorous pentoxide (P_2O_5) prior to the syntheses. Methyl chloroformate were also purified by distillation prior to the syntheses.

Elemental analyses were performed on a Perkin Elmer 2400 CHNS/O Analyzer. Electronic spectra in the 190–1100 nm range were acquired by using a 1.0 cm quartz cuvette in a diode array HP8453 UV/Vis absorption spectrophotometer. Infrared spectroscopy measurements were performed on an Agilent Cary 630 FTIR spectrometer, using the Attenuated Total Reflectance (ATR) method, with a diamond cell. Spectra were recorded from 400-4000 cm^{-1}, with 64 scans and resolution of 4 cm^{-1}.

The ^{1}H and ^{13}C NMR spectra of HIB, PdHIB and PtHIB were recorded in a Bruker Avance III 500 MHz (11.7 T) spectrometer. The {^{15}N,^{1}H} and {^{13}C,^{1}H} correlation NMR spectra were recorded in a Bruker Avance III 400 MHz (9.4 T) spectrometer. Samples were analyzed at 298 K. PdHIB was analyzed in a DMSO-d_6 solution, while PtHIB was analyzed in methanol-d_3 due to its better stability in this solvent. HIB was analyzed in both methanol-d_3 and DMSO-d_6. The chemical shifts for all solution measurements were given relative to tetramethylsilane (TMS). All the ^{13}C and ^{15}N solid state NMR (SSNMR) spectra were recorded in a Bruker 300 MHz spectrometer, using the combination of cross-polarization, proton decoupling and magic angle spinning techniques (CP/MAS) at 10 kHz.

Electrospray ionization mass spectrometry (ESI-MS) measurements were carried out using a Waters Quattro Micro API. Samples were evaluated in the positive mode. Each solution was directly infused into the instrument's ESI source and analyzed in the positive mode, with capillary potential of 3.00 kV, trap potential of 2 kV, source temperature of 150°C and nitrogen gas for desolvation.

3.2. Geometry optimizations

The theoretical calculations of the complexes were carried out using density functional theory (DFT) with a PBE0 hybrid functional [46] and the def2-TZVP basis set [47] for all atoms using ORCA software [48]. The geometric optimization was performed with a convergence criterion of 10^{-5} a.u. for the gradient and 10^{-8} a.u. for the density. The RIJCOSX method [49] was used for the calculation of the exchange energy, using the standard number of points for the grid calculations. The structures were confirmed as the minimum of the potential energy surface (PES) using the same level of theory. Illustrations were rendered using the Pov-Ray tool on Mercury CSD 3.8 (Copyright CCDC 2001-2016) [http://www.ccdc.cam.ac.uk/mercury/].

3.3. Antibacterial assays *in vitro*

Antimicrobial assays were performed in collaboration with Prof. Dr. Wilton Rogério Lustri from the Biological and Health Sciences Department, University of Araraquara (UNIARA). In this study, Gram-positive *Staphylococcus aureus* (ATCC 25923), and Gram-negatives *Escherichia coli* (ATCC – 25922) and *Pseudomonas aeruginosa* (ATCC-27853) bacterial strains were inoculated in tubes containing BHI (Brain Heart Infusion KASVI) and incubated for 18 hours at 35-37 °C. Appropriate amounts of each bacterial suspension were added to new tubes in BHI sterile culture medium until the 1.0 nephelometric McFarland turbidity scale (~$3.0x10^8$ CFU/mL). Volumes of 50 µL of the samples HIB, PdHIB and PtHIB suspended in DMSO (15 $\mu g \cdot \mu L^{-1}$) were added to the second well of the 96 well microplate, followed by the addition of 50 µL of BHI sterile. In the next 6 wells a serial dilution (half) in BHI sterile was performed, maintaining the final volume of 100 µL per well. After that, 100 µL of the bacteria suspensions were added to each serial dilution reaching 0.5 in the McFarland turbidity scale (~$1.5x10^8$ CFU/mL) and the concentrations of the compounds between 3750 $\mu g \cdot mL^{-1}$ and 58.6 $\mu g \cdot mL^{-1}$ for a final volume of 200 µL per well. The first well of the plate was used as control for bacterial growth, containing only the bacteria suspension (~$1.5x10^8$ CFU/mL). The microplates were incubated for 18 h at 35-37 °C in a wet chamber under stirring at 100 rpm. After the incubation time, 15 µL of resazurin 0.02% in sterile aqueous solution were added. The measurements were performed after further incubation for 3 hours[50].

3.4. Antiproliferative assays *in vitro*.

The antiproliferative activities of HIB, PdHIB and PtHIB were investigated over nine human cancer cell lines: U251 (glioma), UACC-62 (melanoma), MCF-7 (breast), NCI-ADR/RES (multidrug resistant ovarian), NCI-H460 (lung, non-small cells), PC-3 (prostate), OVCAR-03 (ovarian), HT-29 (colon), K562 (leukemia). The tumor cell lines were provided by Frederick Cancer Research & Development Center, National Cancer Institute, Frederick, MA, USA, and a non-tumor cell line HaCat (human keratinocyte) used for cell viability was provided by Dr. Ricardo Della Coletta (University of Campinas- UNICAMP, Brazil). The same panel of cells were used previously in other assays performed in our group[51]. Such studies were developed in collaboration with Prof. Dr. Ana Lúcia Tasca Gois, form Chemical, Biological and Agricultural Pluridisciplinary Research Center (CPQBA-UNICAMP, Paulínia, Brazil), where the experiments were performed.

Stock cultures were grown in 5 mL of RPMI-1640 supplemented with 5% fetal bovine serum (RPMI/FBS 5% Gibco®, USA) at 37°C in 5% CO_2 with a 1% penicillin:streptomycin mixture (Nutricell®, Brazil, 1000 U·mL^{-1}) (complete medium)[52,53]. The samples were prepared directly in complete medium (5 mg·mL^{-1}) and then diluted in the same medium, affording the final concentrations of 0.25, 2.5, 25 and 250 µg·mL^{-1}. K_2PdCl_4, K_2PtCl_4 and doxorubicin (final concentrations of 0.025, 0.25, 2.5 and 25 µg·mL^{-1} in complete medium) were used as controls.

Cells in 96-well plates (100 µL cells/well, inoculation density: 3.5 to 6.0 x 10^4 cell/mL) were exposed to different concentrations of sample and controls (100 µL/well) in triplicate, for 48 h at 37°C and 5% of CO_2. Before (T0 plate) and after the sample addition (T1 plates), cells were fixed with 50% trichloroacetic acid, and cell proliferation was determined by the spectrophotometric quantification (540 nm) of cellular protein content using the sulforhodamine B assay[54]. The GI50 values (concentration that inhibits 50% cell growth or cytostatic effect) were determined through non-linear regression, type sigmoidal, analyzed using Origin 8.0 software (OriginLab Corporation, USA)[55].

3.5. Biophysical studies of interaction with DNA

Calf thymus DNA (CT-DNA) was chosen as DNA model as it is widely used in studies of DNA binding anticancer agents that modulate DNA structure and function and because of its predominately double strand form. The CT-DNA was incubated for 24 h at 37 °C (100 $\mu mol \cdot L^{-1}$ CT-DNA aqueous solution in 10 $mmol \cdot L^{-1}$ $NaClO_4$, 1% DMSO), with HIB, $[PdCl_2(HIB)_2]$ and $[PtCl_2(HIB)_2]$ in ratios [compound]/[DNA] of 0.1, 0.2 and 0.3 (10, 20 and 30 $\mu mol \cdot L^{-1}$). The solutions were used for circular dichroism spectroscopic experiments and for the fluorescence experiments with SYBR Green I®. Fluorescence measurements were performed on a Cary Eclipse fluorescence spectrophotometer. Excitation and emission slits were 5 nm and scanning speed was set to medium. A quartz cuvette of four clear windows and optical path length of 1.0 cm was used. SYBR Green I® (SG) was used as fluorescence probe. Excitation wavelength was set as 485 nm and emission window from 505 to 700 nm. For each sample the fluorescence at 520 nm (maximum for SG) was monitored with the consecutive addition of SG (4μL of SG 5x). Circular dichroism (CD) measurements were performed in a Jasco J-720 spectrophotometer, from 205 to 320 nm, with a scanning speed of 20 $nm \cdot min^{-1}$ and 4 accumulations. The Quartz cuvettes of 1.0 cm of optical path length were used.

3.6. Synthesis

3.6.1. Ibuprofen hydrazide (HIB).

The synthesis of the Ibuprofen hydrazide was performed similarly to the methodology described inthe literature by Nakka *et al.*[56] Ibuprofen ($2.0x10^{-3}$ mol, 412.6 mg) was dissolved in 20 mL of dry dichloromethane and 300 μL of trimethylamine (excess) were added to the solution. The solution was stirred for 5 minutes at room temperature and the flask was further transferred to an ice bath. To the cold solution, 200 μL of methyl chloroformate (excess) were added and the solution was kept under stirring for 30 min before being transferred to a flask containing 500 μL of hydrazine hydrate ($H_2NNH_2 \cdot 6H_2O$). This mixture was maintained under stirring and reflux (~50°C) for 3 hours and further 18 hours without heating. Finally, the reaction was quenched with 20 mL of distilled water and the volume of the resulting suspension was reduced under low pressure evaporation. The solid obtained was separated

by filtration, washed with cold water and dried under P_4O_{10}. Anal. Calcd. for $C_{13}H_{20}N_2O$ (%): C, 70.87; H, 9.15; N, 12.72. Found (%): C, 70.99; H, 9.24; N, 12.74. The yield of the synthesis was 71.0%.

3.6.2. PdHIB complex

Potassium tetrachloropalladate(II) ($2.5x10^{-4}$ mol) was first dissolved in a minimum amount of distilled water. To this solution was added HIB ($5.0x10^{-4}$ mol) in 5 mL of methanol. Immediately a yellow solid precipitated and this mixture was kept under stirring for 2 hours. Finally, the solid was collected by filtration, washed with methanol and distilled water and dried under P_4O_{10}. Anal. Calcd. for $PdC_{26}H_{40}N_4O_2Cl_2$ (%): C, 50.53; H, 6.52; N, 9.07. Found (%): C, 50.27; H, 6.48; N, 9.13. The yield of the synthesis was 84.7%. Single light yellow crystals suitable for X-ray diffraction studies were obtained by slow evaporation of an ethanolic solution of the complex.

3.6.3. PtHIB complex.

The synthesis of the platinum complex was similar to that of the palladium(II) one. Potassium tetrachloroplatinate(II) ($2.5x10^{-4}$ mol) was first dissolved in distilled water and then added to a solution of HIB ($5.0x10^{-4}$ mol) in 5 mL of methanol. After a few minutes a yellow solid precipitated and this mixture was kept under stirring for 20 hours. The solid obtained was separated by filtration, washed with methanol and distilled water and dried under P_4O_{10}. Anal. Calcd. for $PtC_{26}H_{40}N_4O_2Cl_2$ (%): C, 44.19; H, 5.71; N, 7.93. Found (%):C, 45.39; H, 5.53; N, 6.97. The yield of the synthesis was 65.8%. No single crystals were obtained even several attempts to perform a full X-ray crystallographic study.

4. Results and discussion

4.1 Single crystal X-ray diffraction

Crystals of PdHIB were obtained by recrystallization in ethanol and its structure was determined by single crystal X-ray diffraction. The crystallographic data are summarized in Table 1 and additional data are presented in Supplementary information (Table S1).

The complex crystallized in the P21/c space group and the asymmetric part of the unit cell is presented in Figure 3(A). As one may observe, the asymmetric unit contains one Pd(II) ion, two chloride ions and two neutral HIB molecules. The complex possess a near perfect square geometry with the least square plane defined by those 4 ligands atoms with r.m.s of 0.0290. The Pd1 ion is deviated 0.0154 Å from the plane defined from N1B, N1A, Cl1 and Cl2. The hydrazide groups of the HIB molecules coordinated *trans* to each other (N1A-Pd-N1B = 178.58(12)°). In addition, two chloride ions complete the coordination sphere (Cl1-Pd-Cl2 = 177.41(3)°).

For similar Pd(II) and Pt(II) compounds reported in the literature[57–62] the *trans* isomers were predicted by DFT calculations to be the most stable geometry, with the exception of the Pt(II) complexes with 4-methoxybenzylcarbazate, benzyl carbazate and 3-methoxybenzoic acid hydrazide[63], in which the *cis* isomers are suggested. This feature indicates that other factors such as steric hindrance, ligand basicity as well as intermolecular interactions may be responsible for the additional stabilization of such system in comparison to *cis*-coordinated complexes.

Table 1. Crystallography data for PdHIB.

Empirical formula	$C_{26}H_{40}Cl_2N_4O_2Pd$
Formula weight ($g \cdot mol^{-1}$)	617.92
T (K)	150
γ(Mo Kα) (Å)	0.71073
Crystal system	Monoclinic
Space group	$P2_1/c$
a (Å)	27.8148 (5)
b (Å)	8.9319 (3)
c (Å)	11.5187 (3)
B	92.462 (2)
V ($Å^3$)	2859.05 (13)
Z	4
D_x ($Mg \cdot m^{-3}$)	1.436
μ (mm^{-1})	0.865
F(000)	1280
Number Par./ Ind. Refl./ R_{int}	361/ 5855/ 0.037
$R[F^2 > 2\sigma(F^2)]$; $wR(F^2)$; S	0.043; 0.103; 1.05
$\Delta\rangle_{max}$ and $\Delta\rangle_{min}$ (e $Å^{-3}$)	1.92 and -1.19

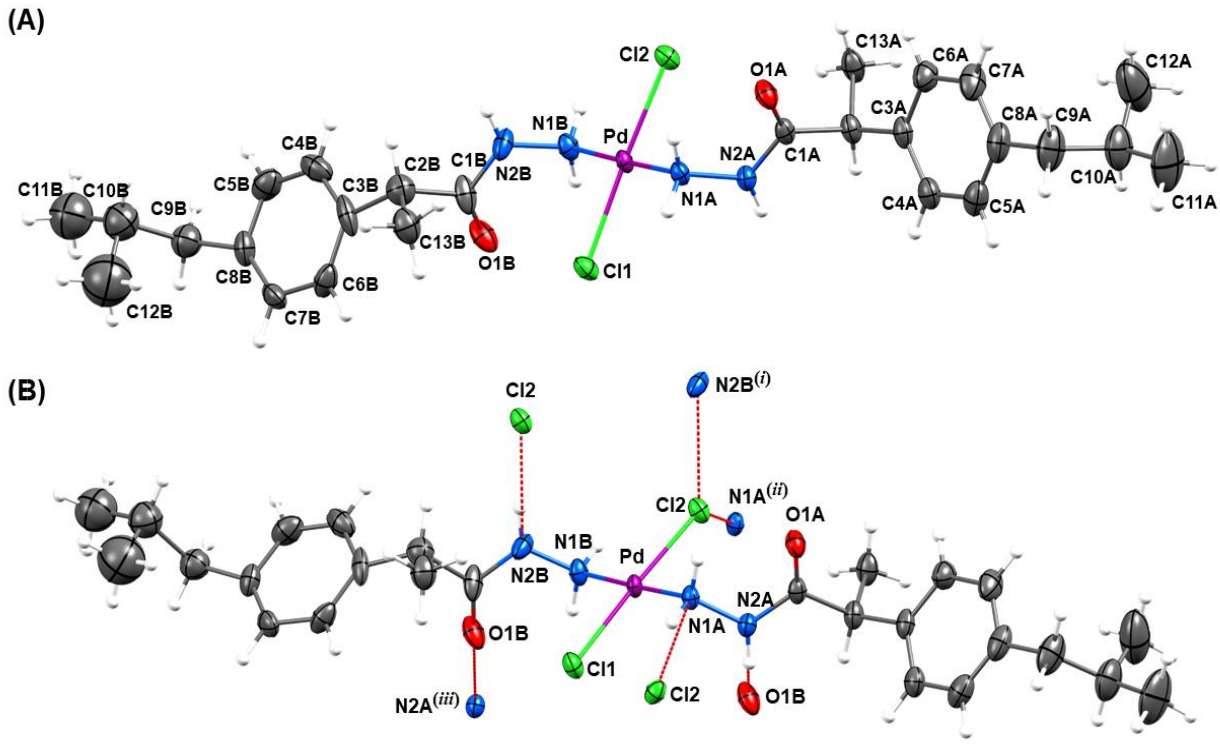

Figure 3. (A) View of asymmetric part of unit cell of the complex PdHIB. (B) Representation of the hydrogen bonds observed among the moieties [symmetry codes:(*i*) 1-x,-y,1-z, (*ii*) x, 1/2-y, -1/2+z, (*iii*) 1-x, 1-y, 1-z]. For clarity, the disorder on the isopropyl group was intentionally not represented. Probability level of ellipsoids: 50%.

An important feature observed in the crystal structure is the presence of both R and S configurations of HIB molecule (related to C2 chiral center) coordinated to Pd(II) ion. Since the ligand was synthesized from a racemic mixture of ibuprofen and no further racemic purification was performed, it is reasonable to suggest that both configurations would be present in the complex.

Moreover, the bond lengths, angles and torsions among Pd(II) and its first sphere of coordination is close to those reported in the literature for a similar structure of palladium(II) complex with 2-thiophenecarboxylic hydrazide (see Supplementary information Tables S2 and S3).[64] Also, the bonds distances and angles from both HIB molecules (of the PdHIB crystal structure) are in good agreement with those observed for ibuprofen and ibuprofenate structures found on The Cambridge Structural Database (CSD) (see Supplementary information Tables S4 and S5).

The presence of chlorine ions contribute to the packing of crystal structure since Cl1 acts as receptor in two hydrogen bonds with N1bi (i=1-x,1-y,1-z) (D…A) (3.365(4)) and N1bii (ii=x,1/2-y,-1/2+z) ((D…A 3.484(4)) atom. The interaction with H1bb ((A…H 3.365(4)) is

forming a dimeric structure with another complex moiety while the interaction with H1ba atom forms a chain in the c direction. Besides it, the Cl2 ion appears as acceptor in other two hydrogen bonds formed with N1Aiii (D…A 3.197(3) iii=x,1/2-y,1/2+z) and N2biv (D…A 3.157(4) iv=1-x,-y,1-z). Finally, the presence of the chlorine ions in the structure play an important role in the packing and stabilization of supramolecular structure. The packing of PdHIB in the crystal structure is shown in the representation of its unit cell (Figure 4). The views of the PdHIB packing through the axis x, y and z are shown in Supplementary information Figure S1.

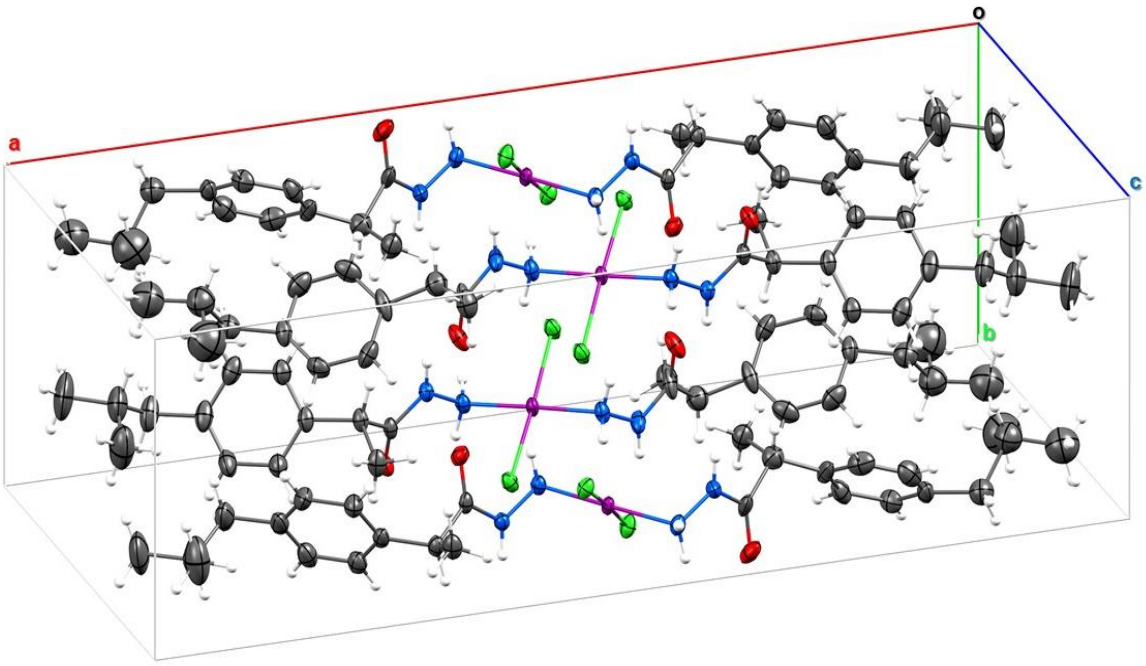

Figure 4. Representation of the unit cell of PdHIB.

4.2 Infrared spectroscopy

The IR spectra of the ligand and the complexes (PdHIB and PtHIB) are shown in Figure 5. The $\delta(NH_2)$ vibrational modes, that appear at 1638 cm^{-1} in the spectrum of the ligand, are no longer observed in the spectra of the complexes due to coordination. Such observations confirm that coordination occurs by the NH_2 [65] as already observed in the crystal structure of PdHIB.

Other important information about coordination were obtained by infrared spectroscopy. For the ligand, the absorption corresponding to ν(N–H) is observed at 3271 cm^{-1} and it is shifted to 3239 cm^{-1} and 3251 cm^{-1} for PdHIB and PtHIB, respectively. It occurs since

coordination to Pd(II) or Pt(II) (Lewis acids) reduces the electron density in the N–H bond (near the coordination site), thus this vibration occurs in lower energy values in the complexes than in the free ligand.

Similarly as discussed above, the ν(C=O) absorption is observed at 1687 cm^{-1} in the ligand and it is shifted to 1668 cm^{-1} in the PdHIB spectrum and to 1666 cm^{-1} for PtHIB due to change of electron density induced by coordination. The region between 2960 and 2850 cm^{-1}, which contains the ν(C–H) stretches, is identical in all three spectra, since the coordination occurs in a nitrogen far from C–H bonds.[65,66]

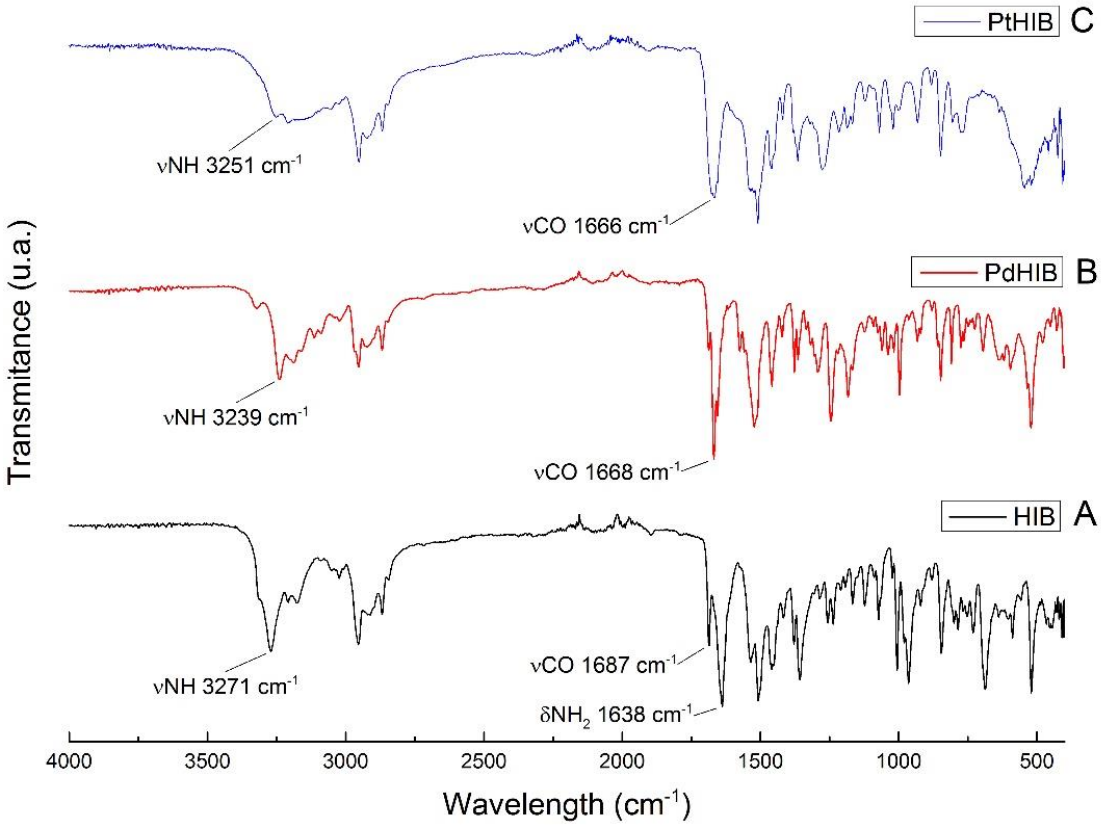

Figure 5. Infrared spectra of HIB (A), PdHIB (B) and PtHIB (C).

4.3 Thermogravimetric and differential thermal analyses (TG/DTA)

Thermogravimetric (TGA) and differential thermal analyses (DTA) were performed in oxidant atmosphere and the data obtained are shown in Figure 6. For the PdHIB complex the loss of two ligands plus 2Cl^- ions is observed from 130°C to 450°C. Calc. for loss of 2 HIB

plus 2Cl ligands (%) 82.7; found (%) 80.2. The percentage of residue is coherent with Pd°. Calc. for Pd° (%) 17.3; found (%) 19.8.

Similarly, the profile of the TG/DTA curves of PtHIB shows the loss of the two HIB ligands between 122°C and 375°C. Calc. for loss of 2 HIB plus 2 Cl ligands (%) 72.4; found (%) 70.2. The percentage of residue is coherent with Pt°. Calc. for Pt° (%) 27.6; found (%) 29.2.

These results reinforce the composition of the complexes suggested by elemental analyses, being $[PdCl_2(C_{13}H_{20}N_2O)_2]$ and $[PtCl_2(C_{13}H_{20}N_2O)_2]$.

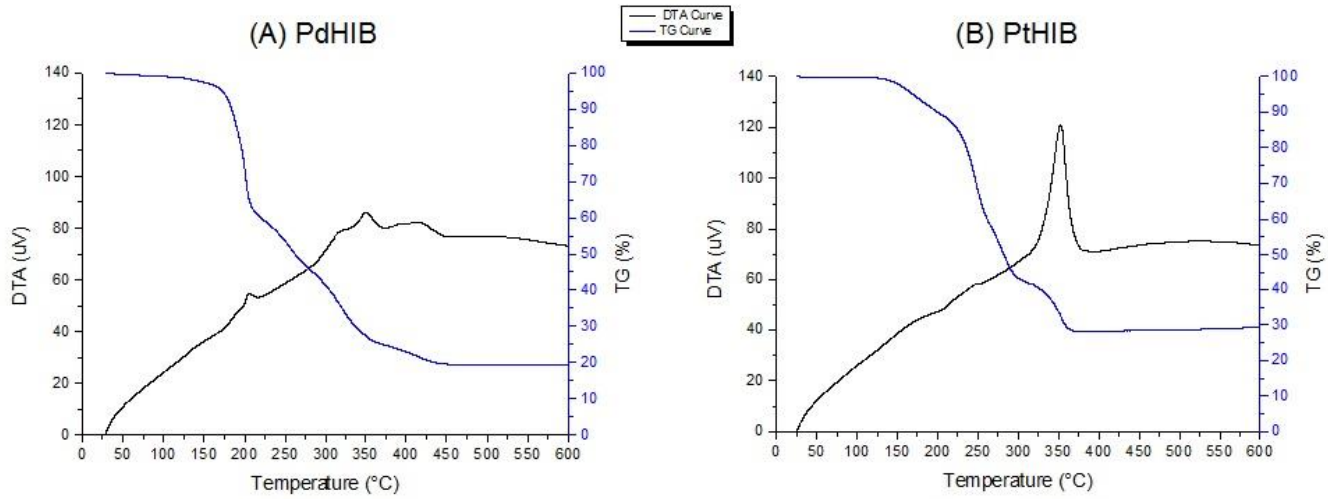

Figure 6. TG (blue) and DTA (black) curves for PdHIB (A) and PtHIB (B)

4.4 Stability in solution

The UV-Vis spectra of the ligand HIB in methanol shows an intense absorption band with a maximum at 227 nm. In the same region, there are bands from the ligand in PdHIB and PtHIB, as presented in Figure 7.

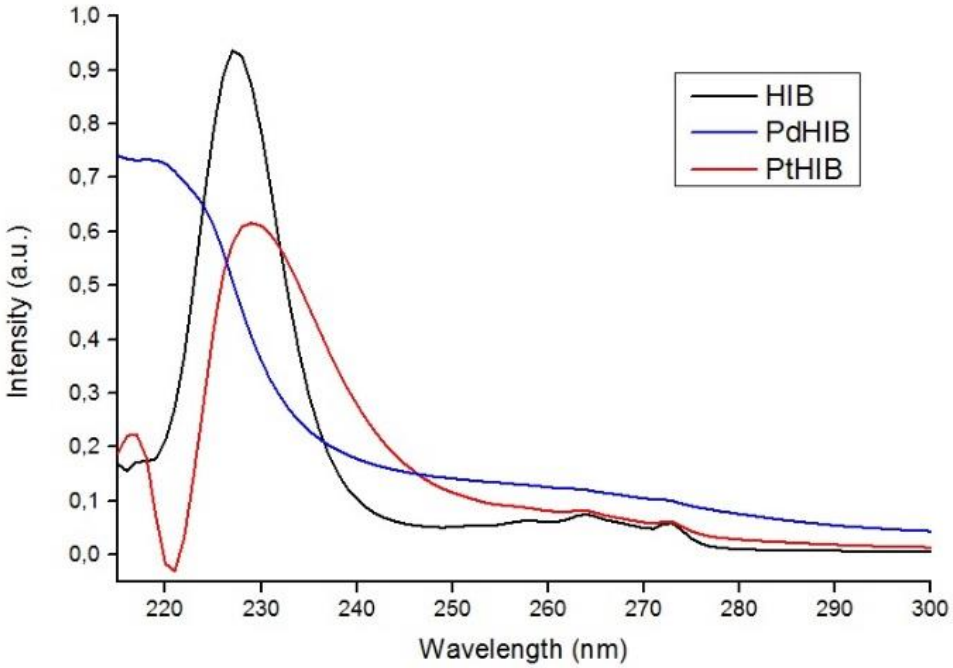

Figure 7. UV spectra of HIB, PdHIB and PtHIB in methanol.

The UV-Vis spectroscopy was used to evaluate the stability of PdHIB and PtHIB in solutions of DMSO and methanol. The spectra were recorded every 30 minutes for 22 hours in the wavelength range of 200-400 nm and they are presented in Figure 8. The solutions in methanol and DMSO are in concentrations of 133 $\mu mol \cdot L^{-1}$ and 200 $\mu mol \cdot L^{-1}$, respectively. The spectra in DMSO are presented in a different range due to the DMSO interference.

It was determined that PtHIB is not stable in DMSO (Figure 8C), as there were significant changes the spectrum noticed by the maximum absorbance that increased from 0.8 to values higher than 1.0, probably because of ligand exchange. This is not observed in the kinetic studies of the other samples shown in Figure 8.

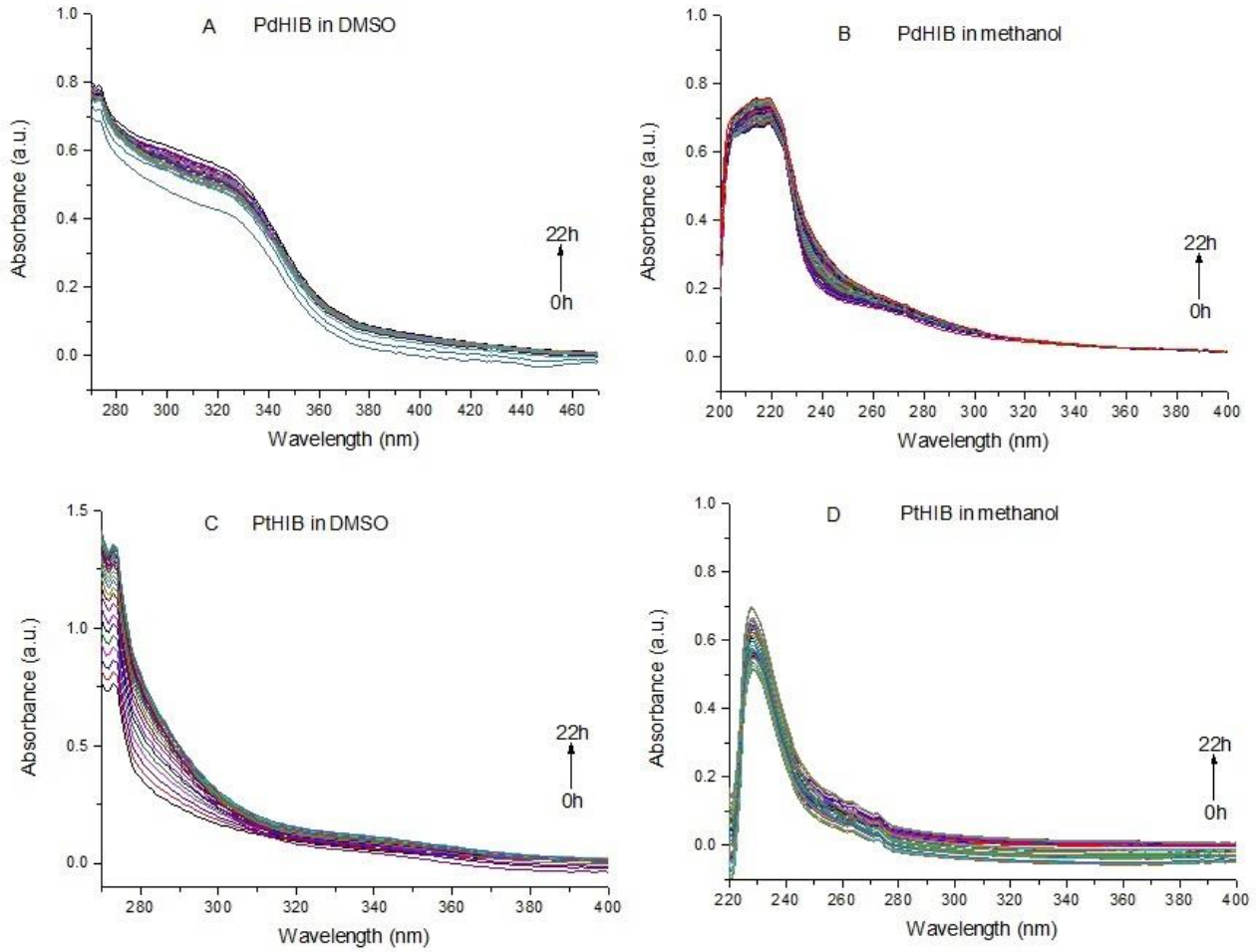

Figure 8. UV-Vis spectra of PdHIB in DMSO (A), PdHIB in MeOH (B), PtHIB in DMSO (C) and PtHIB in MeOH (D) in the time range from 0 to 22 hours.

4.5 NMR spectroscopy

The characterization of the ligand and complexes was also performed by solution NMR, including ^{1}H, ^{13}C, {^{13}C,^{1}H} HSQC (heteronuclear single quantum coherence), {^{13}C,^{1}H} HMBC (heteronuclear multiple bond coherence), {^{15}N,^{1}H} HSQC and {^{15}N,^{1}H} HMBC NMR in DMSO-d_6 and methanol-d_4. In addition, ^{15}N and ^{13}C solid state NMR using CP-MAS (cross polarization and magic angle spinning) technique were also applied to the study of the complexes.

In the ^{1}H NMR spectrum of HIB in DMSO-d_6 it was possible to see the signals of the hydrogen atoms bonded to the nitrogen atoms (Figure 9) that were confirmed by {^{15}N,^{1}H} HSQC (Figure 10). The integrated intensity of these hydrogens signals are also in agreement

with two hydrogens for NH_2 (Relative intensity = 1.89) and one hydrogen for NH (Relative intensity = 0.94).

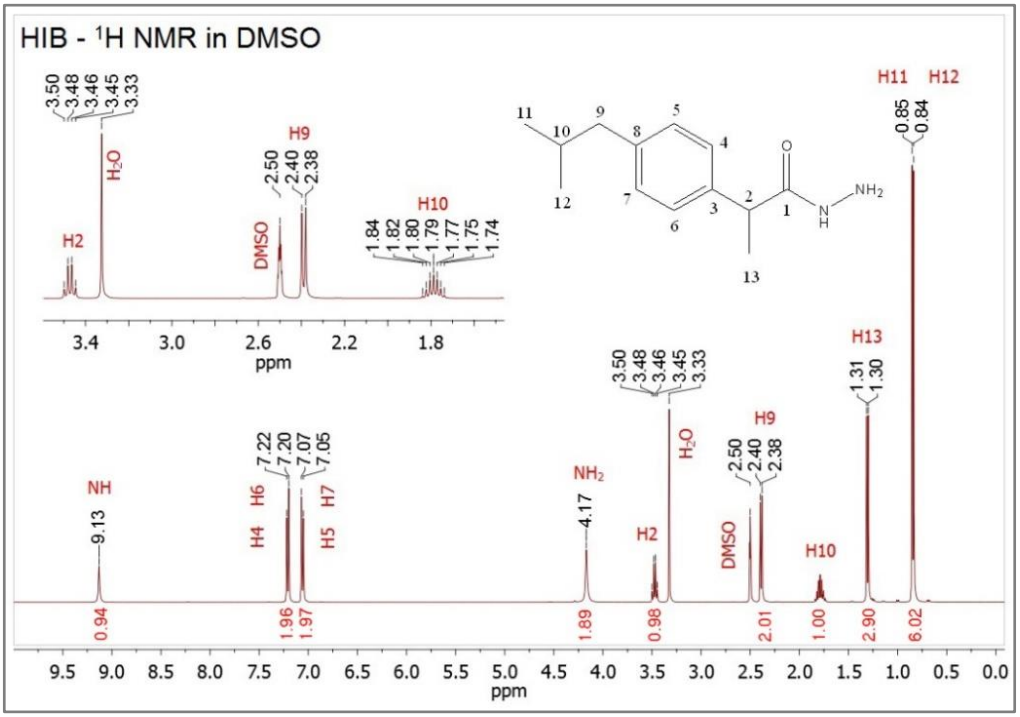

Figure 9. ^{1}H NMR spectrum of HIB in DMSO-d_6. On top of the peaks are shown the chemical shifts and at the bottom are the integrated intensities. An expansion from 1.7 to 3.5 ppm is presented on the top left corner.

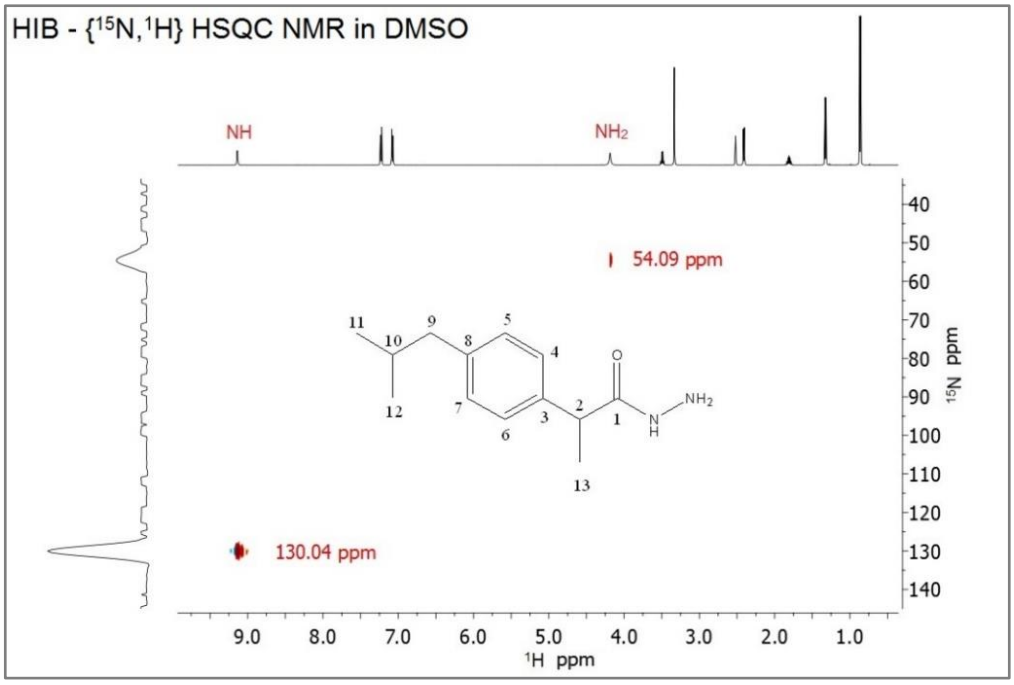

Figure 10. $\{^{15}N,^{1}H\}$ HSQC NMR spectrum of HIB in DMSO. The chemical shifts of the nitrogen atoms are shown.

Figures 11-13 show the ^{1}H, $\{^{13}C,^{1}H\}$ HSQC and $\{^{13}C,^{1}H\}$ HMBC NMR spectra of HIB in Methanol-d_6 (MeOD) with the attributions of all the C and H atoms. Carbons named C3 and C8 were unequivocally assigned by the $\{^{13}C,^{1}H\}$ HMBC technique. It was possible because in this spectra C3 has multiple bond correlations to H13 and H2, while C8 correlates to H9. The hydrogens of the groups NH and NH_2 are not observed in MeOD solution because they are able to exchange with the deuterium of the hydroxyl group due to their lability, therefore broadening the signal. It does not happen in DMSO-d_6 solution as this solvent lacks a more labile hydrogen.

Also, note that hydrogens H4 and H6 are equivalent by symmetry, as are the pairs H5-H7 and H11-H12 in all the ^{1}H NMR because of the free rotation of the aromatic ring and isopropyl group in solution.

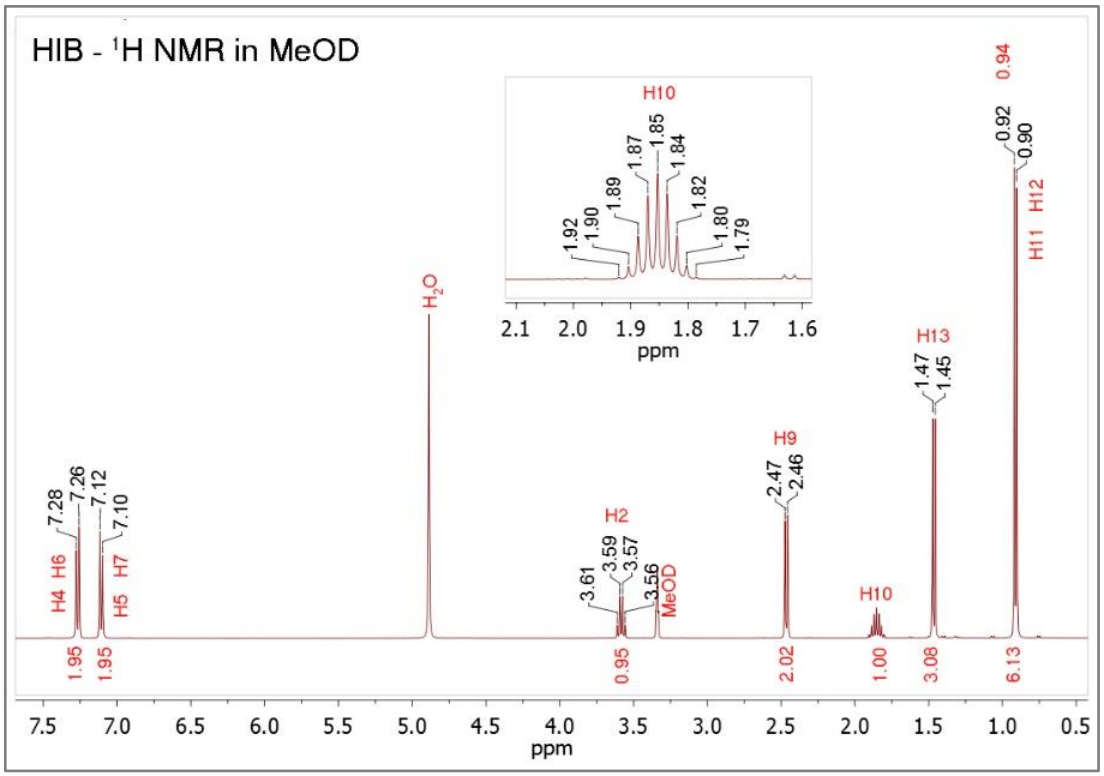

Figure 11. ^{1}H NMR spectrum of HIB in MeOD. On top of the peaks are shown the chemical shifts and in the bottom are the calculated integrals. An expansion from 1.6 to 2.1 ppm highlights the signal of the hydrogen H10.

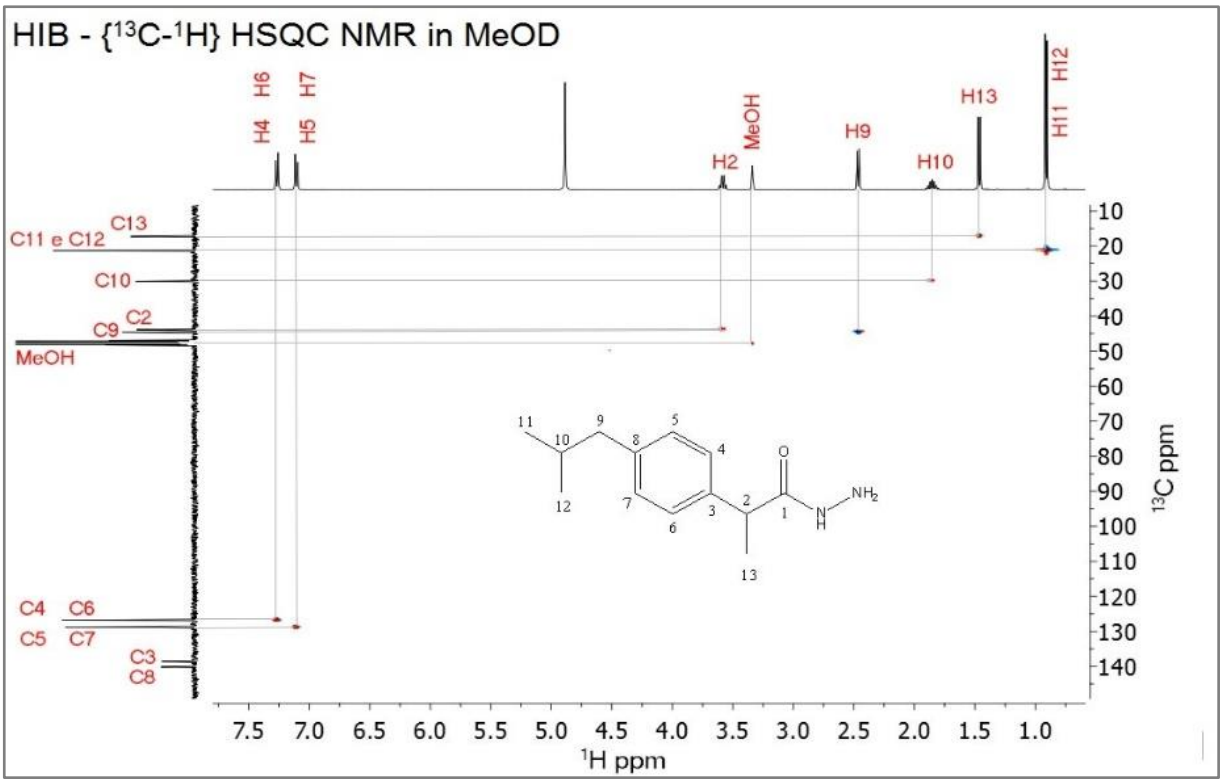

Figure 12. NMR spectrum of HIB {^{13}C,^{1}H} HSQC in MeOD.

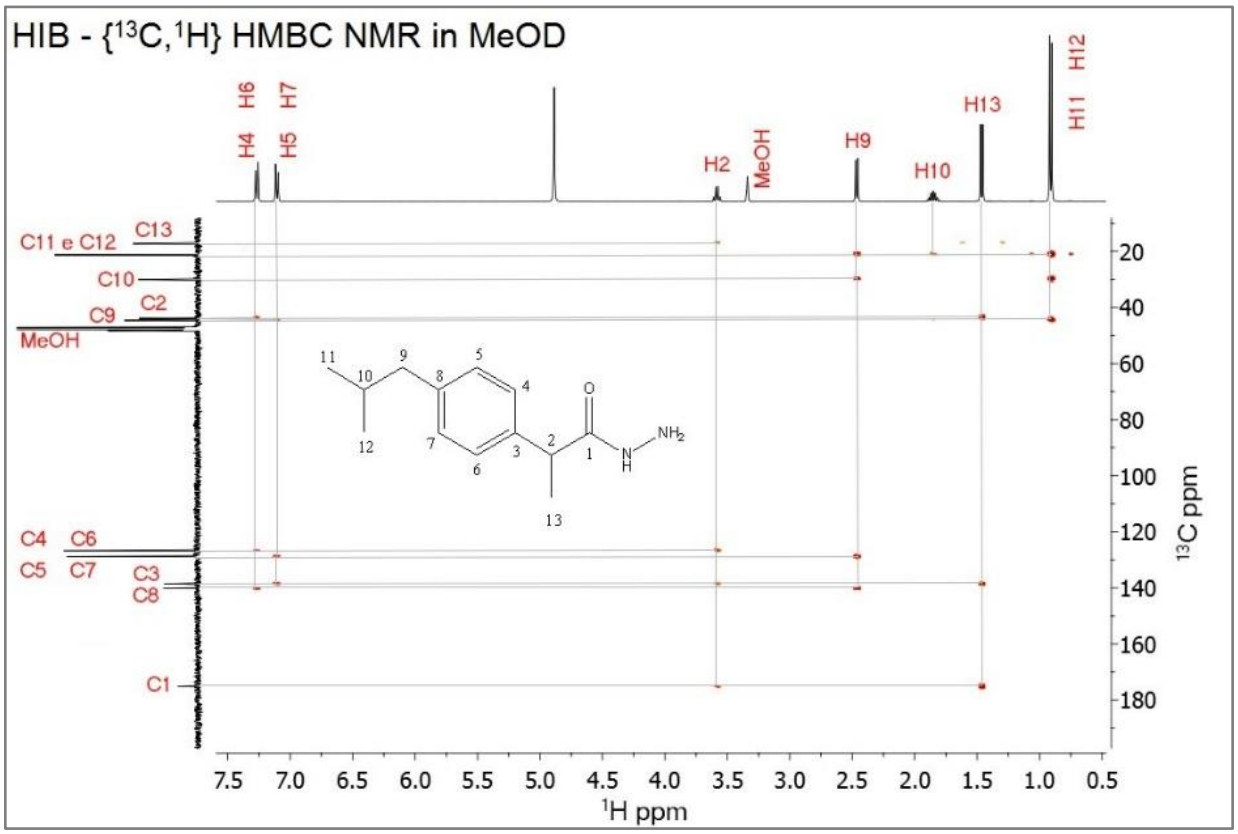

Figure 13. NMR spectrum of HIB {^{13}C,^{1}H} HMBC in MeOD.

It was observed that PdHIB and PtHIB behave differently in solution, as expected. The PtHIB NMR spectrum in DMSO-d_6 shows decomposition of the complex within few minutes, while PdHIB was stable in DMSO-d_6 even after 10 days, which confirms the stability suggested in the UV-Vis experiments. Figure 14 shows the {^{13}C,^{1}H} HMBC NMR spectrum of PdHIB in DMSO-d_6 and Figure 15 shows the equivalent spectrum for PtHIB in MeOD.

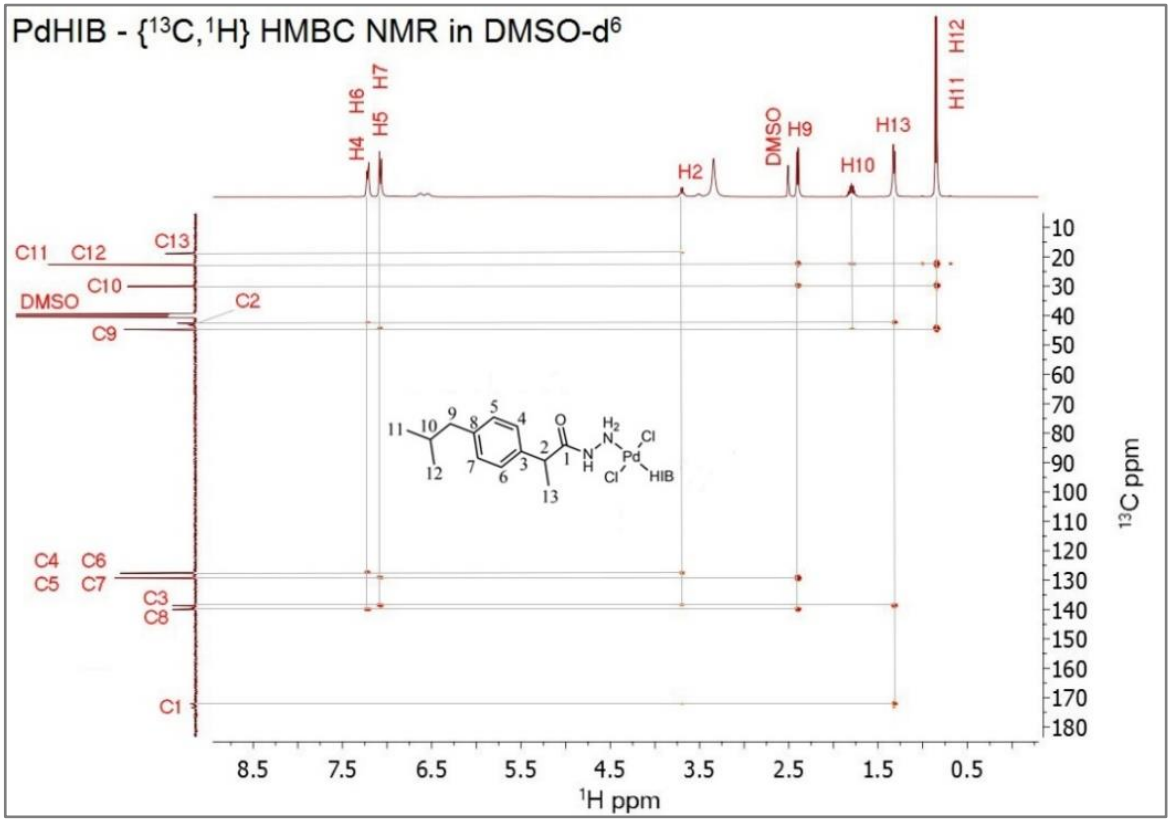

Figure 14. NMR spectrum of PdHIB {^{13}C,^{1}H} HMBC in DMSO-d_6.

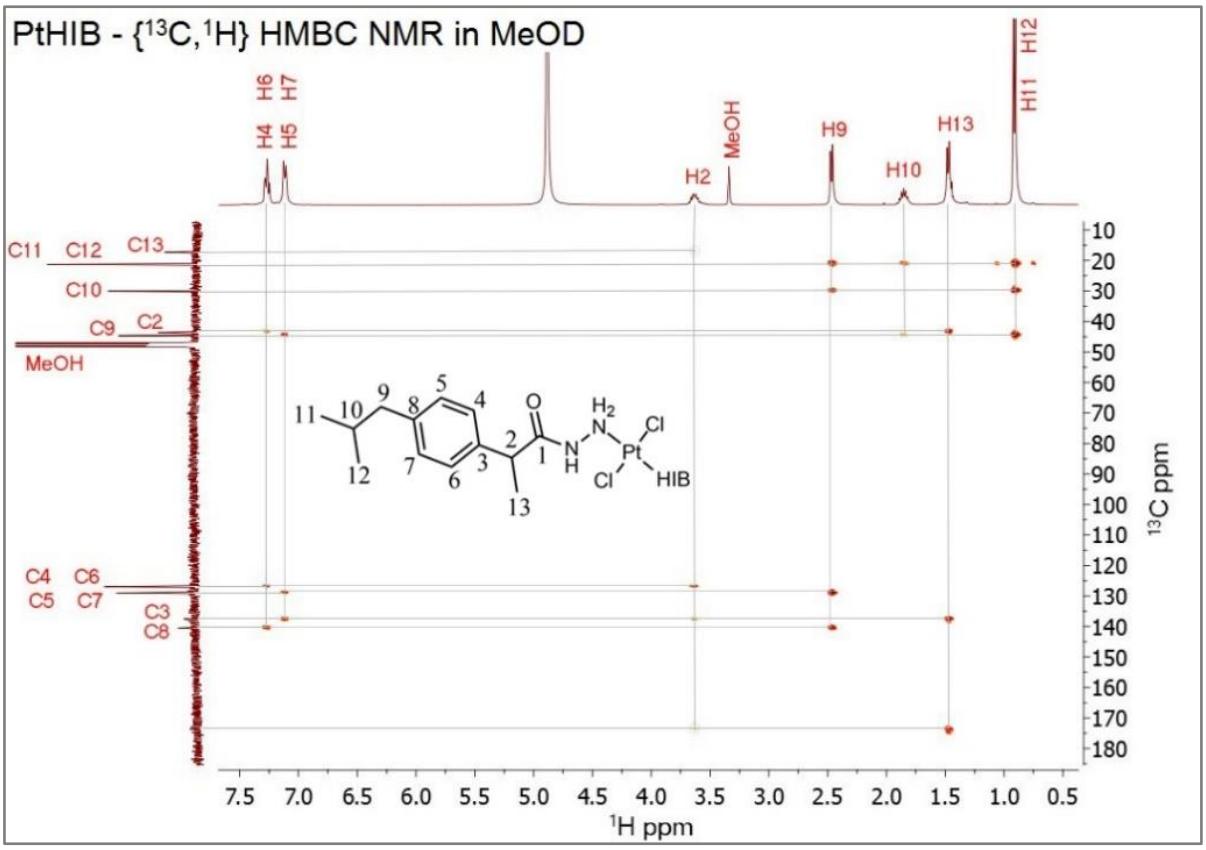

Figure 15. NMR spectrum of PtHIB {^{13}C,^{1}H} HMBC in MeOD.

The use of solid state NMR was necessary to characterize the complexes as the nitrogen atoms could not be observed in solution. Furthermore, the analysis in the solid state gave a fair representation of both complexes, independent of the solvents. Table 2 shows the chemical shift in the ^{13}C and ^{15}N SSNMR spectra of HIB, PdHIB and PtHIB.

Table 2. Chemical shifts in the ^{13}C and ^{15}N SSNMR for HIB, PdHIB and PtHIB.

Chemical shifts (ppm)											
	Carbon numbers									Nitrogen atoms	
	13	11/12	10	2	9	4 /5/6 /7	3	8	1	NH	NH_2
HIB	17.3	24.8	31.7	43.6	46.6	129.9	140.9	140.9	179.6	127.2 134.4	56.3
PdHIB	19.9	23.8	31.0 31.9	44.2	45.0	128.6	138.3	139.9	175.0	131.1 136.0 139.5	11.7 18.1
PtHIB	18.2	22.7	30.4	45.1	45.1	129.2	139.6	139.6	173.5	138.1	9.7

The main difference in chemical shifts between the spectrum of HIB and the spectra of the complexes is in the nitrogen of the NH_2 group, which is shifted from 56.3 ppm for HIB to 11.7-18.1 ppm for PdHIB and 9.7 ppm for PtHIB as presented in Figure 16. This is an evidence that coordination to Pd(II) and Pt(II) occurs by the NH_2 of the hydrazide group.

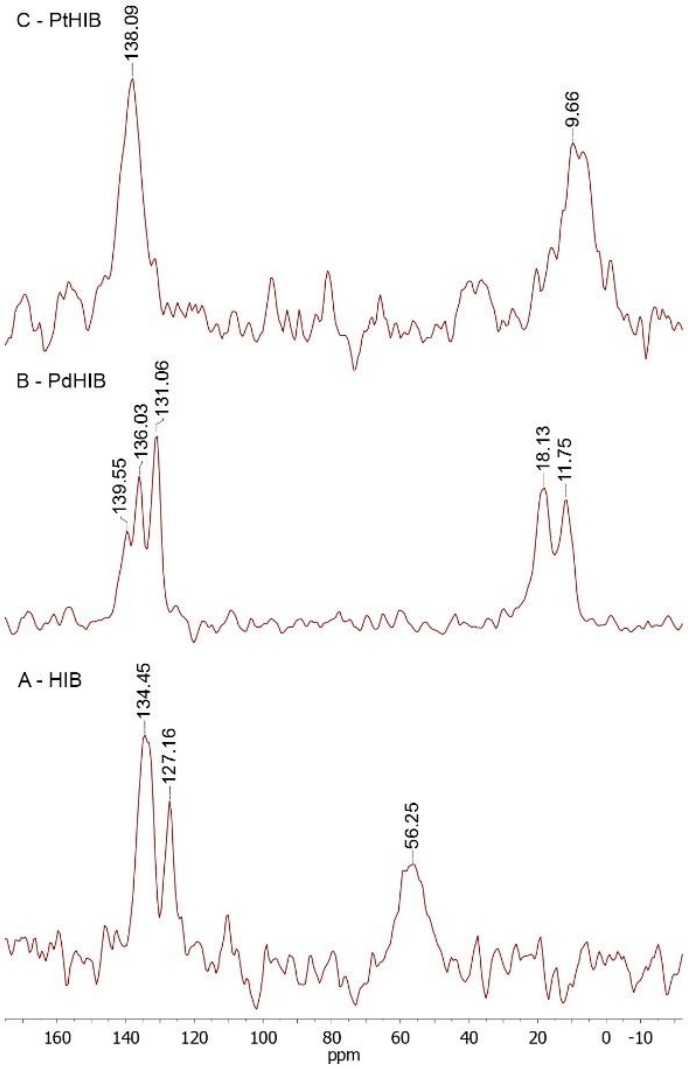

Figure 16. ^{15}N SSNMR spectra of HIB (A), PdHIB (B) and PtHIB (C).

4.6 Mass spectrometric measurements

The mass spectrum of PdHIB (Figure 17) presents the ion $[Pd(HIB)_2Cl]^+$ at *m/z* 583.1874 (error 32.6 ppm) as the most intense peak, but it also shows the ion $[Pd(HIB)_2 - H]^+$ at *m/z* 545.2149, which refers the complex with one of the ligands bearing a negative charge due to deprotonation. Furthermore, the signal at m/z 221.1735 corresponding to the protonated ligand $[HIB+H]^+$ is observed. Additional patterns of species containing Pd ions are also present, such as $[Pd(HIB)_3Cl]^+$ at m/z 801.3544, $[Pd_2(HIB)_3 - 3H]^+$ at m/z 871.2578, $[Pd_2HIB_3Cl - 2H]^+$ at m/z 907.2196 and $[Pd_2HIB_3Cl_2 - H]^+$ at 943.2081.

For PtHIB complex (Figure 18) the results are similar, with the ions $[Pt(HIB)_2Cl]^+$ at *m/z* 671.2528 (error 9.2 ppm), $[Pt(HIB)_2 - H]^+$ at *m/z* 634.2934, $[Pt(HIB)_2 - H + DMSO]^+$ at m/z

712.2815 and $[Pt(HIB)_3 - H]^+$ at m/z 854.4240. The signal corresponding to the protonated ligand is also observed.

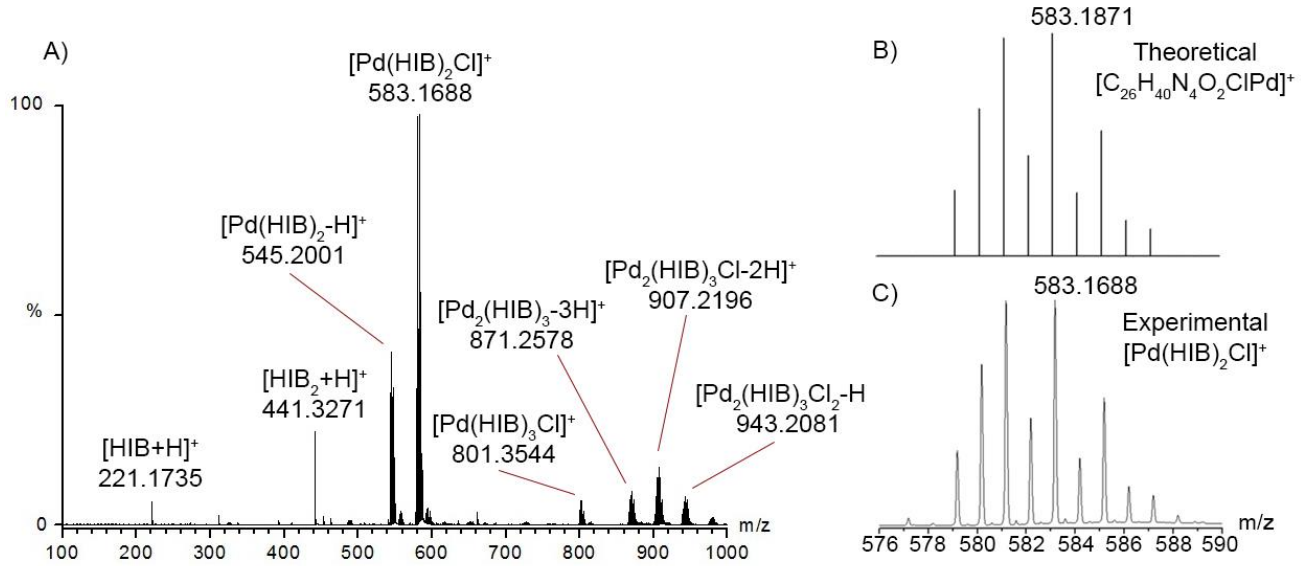

Figure 17. (A) Mass spectra for the PdHIB complex from 100 to 1000 m/z. (B) Theoretical isotope pattern for the complex $[Pd(HIB)_2Cl]^+$. (C) ESI(+)-QTOF mass spectrum of PdHIB from 576 to 590 m/z.

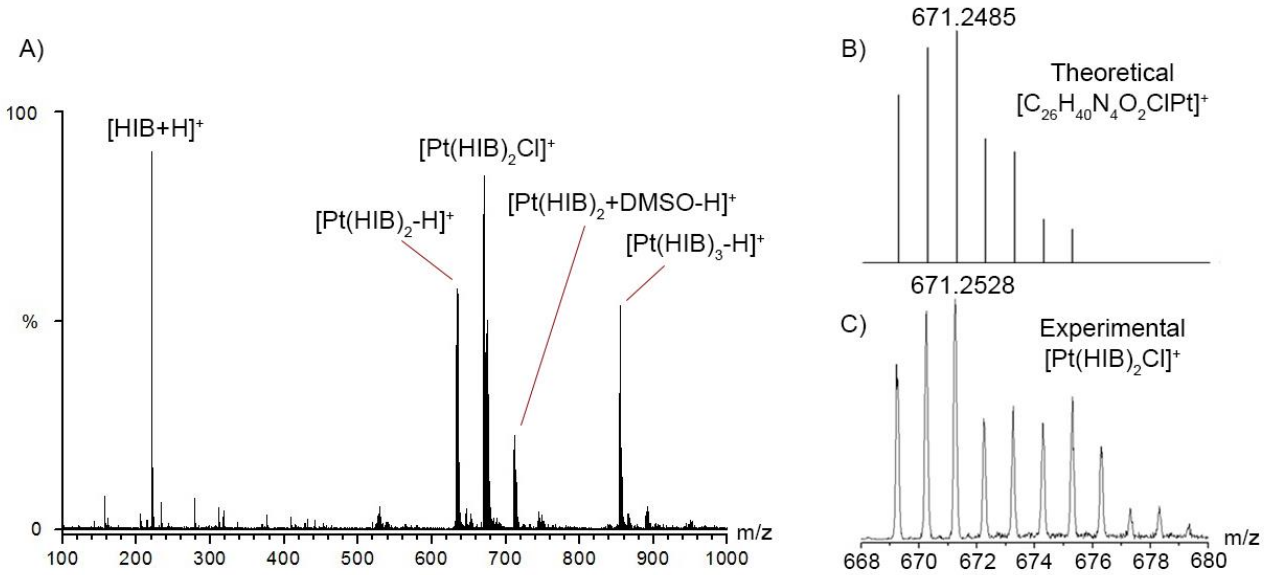

Figure 18. (A) Mass spectra for the PtHIB complex from 100 to 1000 m/z. (B) Theoretical isotope pattern for the complex $[Pt(HIB)_2Cl]^+$. (C) ESI(+)-QTOF mass spectrum of PtHIB from 668 to 680 m/z.

4.7 DFT calculations

The geometric calculations for PdHIB and PtHIB complexes were optimized using density functional theory (DFT). The DFT data, including the atomic coordinates for the optimized structures, are presented in Supplementary Information - Tables S6 and S7.

As previously observed, the crystal structure of the Pd(II) complex is composed of one Pd(II) coordinated by two neutral HIB molecules and two chloride ions. The elemental analysis, as well as the ESI-QTOF-MS of the Pd(II) complex in its powder form, indicate that the same composition is observed in the crystal and powder samples. In addition, the same studies regarding the Pt(II) complex indicate that it also possesses a 1:2:2 metal/HIB/chloride ratio, as observed for the Pd(II) complex. Moreover, the SSNMR and IR spectroscopic measurements of the powder samples indicate that, for both complexes, the coordination occurs by the hydrazide moieties of HIB. Therefore, it is reasonable to assume that the Pt(II) complex is coordinated by HIB in the same fashion as observed in the PdHIB crystal structure. The DFT optimized structure of PtHIB and PdHIB are represented in Figures 19 and 20.

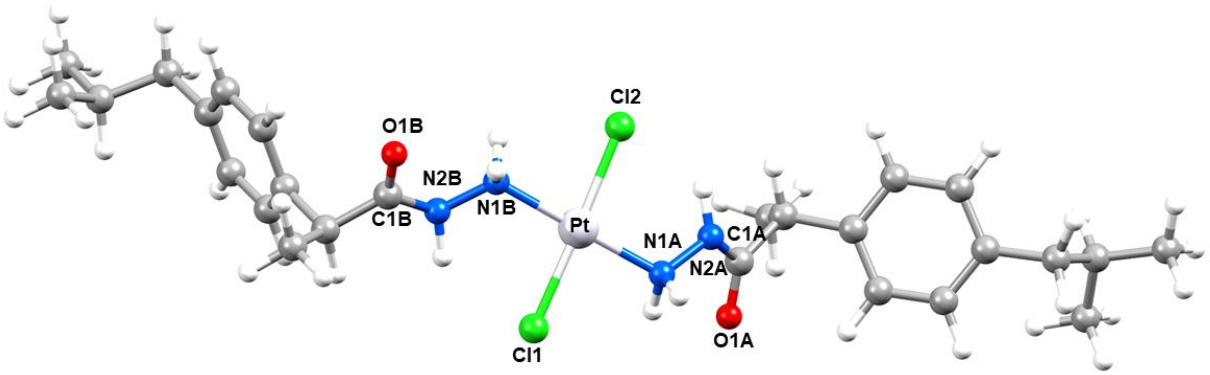

Figure 19. PBE0/def2-TZVP optimized structure of $[PtCl_2(HIB)_2]$.

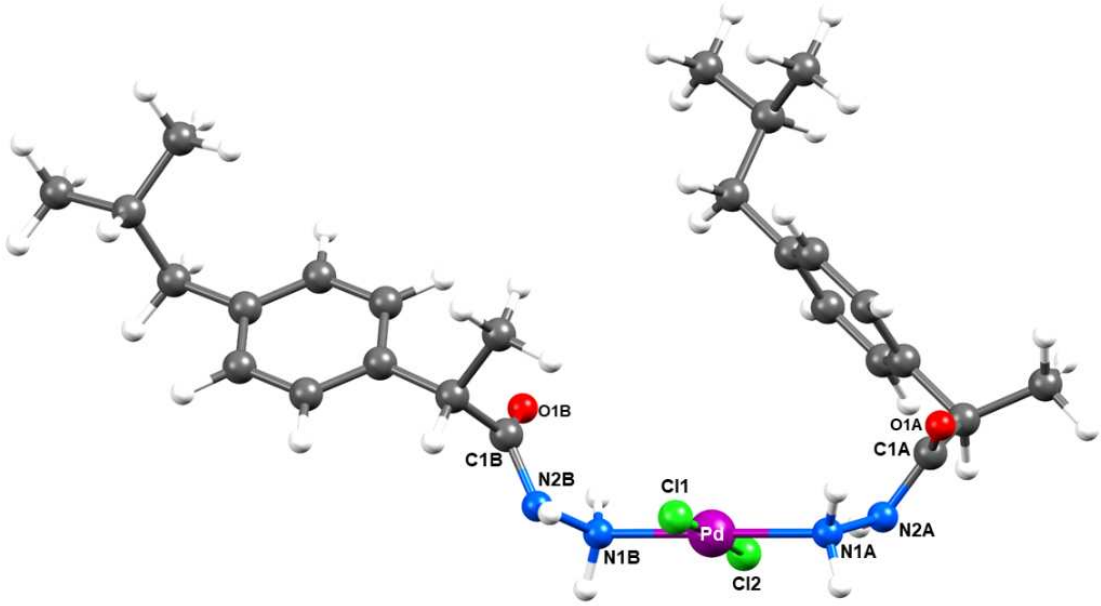

Figure 20. PBE0/def2-TZVP optimized structure of $[PdCl_2(HIB)_2]$.

In a different way of the optimized structure of the Pt(II) complex, in which the HIB molecules are arranged in a similar fashion to PdHIB crystal structure, the HIB ligands on DFT optimized structure of the Pd(II) complex are arranged at different positions (see Figure 21). The planes formed among the carbon atoms of the benzyl ring of the HIB molecules in the crystal structure are observed displaced by 80.15° and 30.07° of their respective planes in the DFT optimized structure. Since intermolecular interactions are observed in the crystal structure that could not be otherwise simulated by the DFT model (which considers a single molecule in vacuum), it is reasonable to assume that the most thermodynamically stable structure obtained by DFT can be different to that observed in the crystal.

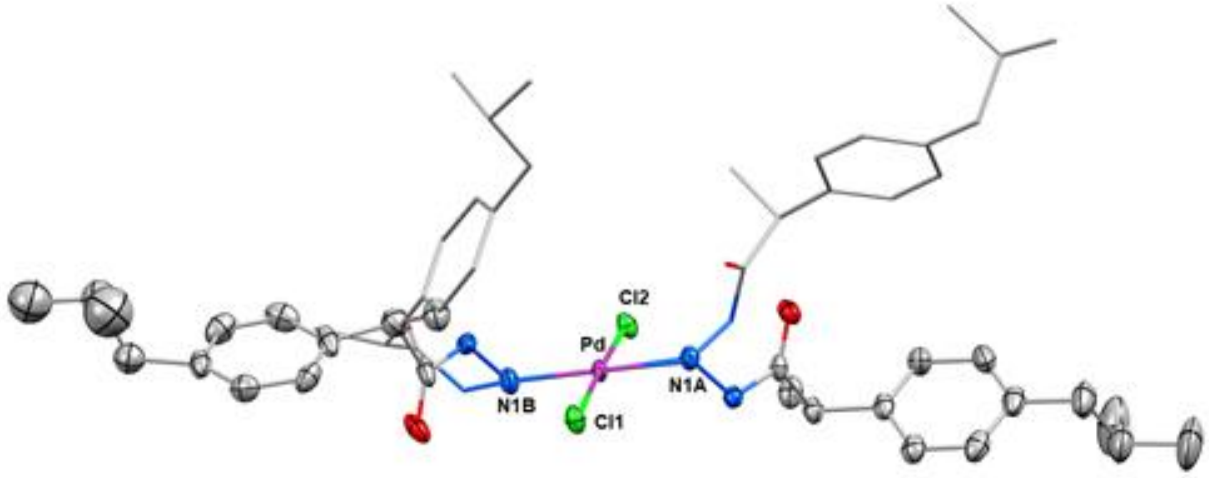

Figure 21 - Comparison between the crystal structure of $[PdCl_2(HIB)_2]$ and its optimized structure by DFT. The structures were overlapped considering the common positions of the metal ion and its first coordination sphere. The crystal structure is represented as ellipsoids and the DFT structure is represented as sticks. The hydrogen atoms were intentionally omitted.

Apart from this difference between crystal structure of PdHIB and its optimized structure by DFT, both optimized structures of Pd(II) and Pt(II) complexes possess HIB ligands with bond lengths and angles similar to those observed in the crystal structure of the Pd(II) complex (see Supplementary information - Table S8). Furthermore, as one may observe in Table 3, the bond distances for Pd(II) and the ligand atoms are very close to the values observed in the crystal structure. On the other hand, for PtHIB the same selected bonds were compared to the crystal structure of a similar complex previously reported in the literature (dichloro(1,6-diaminotetrahydropyrrolo[2,3-b]pyrrole-2,5(1H,4H)-dione)platinum(II))[67]. Again, the bond lengths for the Pt(II) complex are very close to those observed in the literature.

The DFT optimized structures of PdHIB and PtHIB were also compared with other DFT optimized structures found in the literature for Pd(II) and Pt(II) complexes that have NH_2 moieties coordinated in trans geometry (Table 3). It is interesting to notice that in these complexes the Pd-N bond lengths calculated using the PBE0 hybrid functional are very similar to each other and to the distances reported in the crystal structures. On the other hand, the same lengths calculated using the B3LYP functional are generally longer, suggesting that the functional PBE0 better predicts this kind of coordination bond.

Table 3. Selected bond lengths for the Pd(II) and Pt(II) complexes in comparison to the literature and to the crystal structure of $[PdCl_2(HIB)_2]$. The bond lengths calculated by DFT are presented in average.

	M-Cl2/ M-Cl1*	**M-N1B/ M-N1A**	**N1B-N2B/ N1A-N2A**	**C1B-O1B/ C1A-O1A**
$[PdCl_2(HIB)_2]$ crystal	2.2889(9)/ 2.309(1)	2.048(3)/ 2.036(3)	1.408(4)/ 1.425(4)	1.226(5)/ 1.224(4)
$[PdCl_2(HIB)_2]$ DFT	2.307‡	2.046‡	1.406‡	1.214‡
$[PdCl_2(C_{10}H_{12}N_2)_2]$ [58]	2.337‡	2.049‡	-	-
$[PdCl_2(L)_2]$** [61]	2.34‡	2.07‡	-	-
$[Pd(C_6H_{10}NO_3S)_2]$ [60]	-	2.089†	-	-
$[Pd(C_{11}H_{11}N_2O_2)_2]$ [57]	-	2.08†	-	-
$[Pd(C_6H_{10}NO_2S)_2]$ [59]	-	2.11†	-	-
Pt(II) complex§ crystal	2.296(2)/ 2.299(2)	2.051(5)/ 2.028(6)	1.416(8)/ 1.419(9)	1.227(5)/ 1.210(9)
$[PtCl_2(HIB)_2]$ DFT	2.308‡	2.049‡	1.407‡	1.215‡
$[Pt(C_{11}H_{11}N_2O_2)_2]$ [62]	-	2.08†	-	-

* M refers to the dicationic metal ion, M(II) (i.e. Pd(II) or Pt(II)).

** L refers to carbazates and hydrazides (mean value).

§ Z. Kristallogr. 209 (1994) 293.[67]

‡ calculated using the PBE0 functional

† calculated using the B3LYP functional

4.8 Biological assays

4.8.1 Minimal inhibitory concentration (MIC)

The PdHIB and PtHIB complexes were not able to inhibit the growth of any bacteria in the concentrations tested. However, HIB was able to inhibit *S. aureus* (ATCC 25923) and *E. coli* (ATCC – 25922) in the MICs of 1850 $\mu g \cdot mL^{-1}$ and 3750 $\mu g \cdot mL^{-1}$, respectively. These results are interesting since free ibuprofen does not possess any antibacterial activity, but when the COOH group is replaced by a $CONHNH_2$ group the compound is active. The fact that the complexes do not possess antibacterial activities may indicate that free $CONHNH_2$ group is determinant for the antibacterial activity, since the coordination occurs by this group and the complexes are inactive.

4.8.2 Antiproliferative assays

The antiproliferative activities of HIB as well as PdHIB and PtHIB complexes were evaluated over a panel of human tumor cells. Doxorubicin, a frontline drug used for the treatment of several types of cancer [68], was used as positive control and the precursor salts, $K_2[PdCl_4]$ and $K_2[PtCl_4]$, were also evaluated. This activity was expressed as the parameter GI_{50} representing the sample concentration necessary to inhibit 50% of cell growth, therefore a low GI_{50} means a high antiproliferative activity. The results are reported by estimated concentration ($\mu mol \cdot L^{-1}$) (Table 4), as the compounds were suspended in water and added to the biological medium (no DMSO was used to improve PdHIB and PtHIB solubility).

The Pt(II) complex presented GI_{50} values higher than 353.2 $\mu mol \cdot L^{-1}$ for all the cell lines. On the other hand, the PdHIB complex showed selective inhibition against the ovarian cancer cell line (OVCAR-03, GI_{50} = 27.0 $\mu mol \cdot L^{-1}$) (Table 4). Another important aspect of antiproliferative activity is the selectivity towards cancer and normal cells. Experimentally, this selectivity can be estimated using a selectivity index (SI), defined as [69]:

$$\mathrm{SI} = \frac{\mathrm{GI}_{50\ (HaCat)}}{\mathrm{GI}_{50\ (cancer\ cell\ line)}}$$

Where $GI_{50\ (HaCat)}$ is the GI_{50} for the non-tumor human cell line (immortalized keratinocytes) and $GI_{50\ (cancer\ cell\ line)}$ is the GI_{50} value for a given cancer cell line. Hypothetically, the higher the value of SI the higher the dose that could be administered safely [69]. The values of SI calculated for each cell line are presented in Table 4. Antiproliferative profiles are presented in the Supplementary information - Figures S2 - S7.

Table 4. GI_{50} (μmol·L^{-1}) and selectivity index (SI) values obtained for HIB, $[PdCl_2(HIB)_2]$, $[PtCl_2(HIB)_2]$, $K_2[PdCl_4]$, $K_2[PtCl_4]$ and doxorubicin in the *in vitro* antiproliferative assay.

GI_{50} (μmol·L^{-1})

	U251	UACC-62	MCF-7	NCI-ADR/RES	NCI-H460	PC-3	OVCAR-03	HT-29	K562	HaCat
HIB	511.10	144.34	171.12	*	*	521.54	92.14	*	119.83	217.42
PdHIB	*	*	*	*	*	*	27.02	*	*	>404.6
PtHIB	*	*	*	*	*	*	*	*	*	353.24
K_2PdCl_4	99.25	10.72	96.50	90.68	117.94	96.80	11.33	96.80	85.16	82.71
K_2PtCl_4	64.08	4.09	61.91	20.23	57.81	20.71	23.37	66.49	59.02	6.99
Doxo	<0.045	<0.045	<0.045	0.46	<0.045	0.42	0.092	0.26	0.055	<0.045

Selectivity Index (SI)

	U251	UACC-62	MCF-7	NCI-ADR/RES	NCI-H460	PC-3	OVCAR-03	HT-29	K562
HIB	0.43	1.51	1.27	*	*	0.42	2.36	*	1.81
PdHIB	*	*	*	*	*	*	>14.97	*	*
PtHIB	*	*	*	*	*	*	*	*	*
K_2PdCl_4	0.83	7.71	0.86	0.91	0.70	0.85	7.30	0.85	0.97
K_2PtCl_4	0.11	1.71	0.11	0.35	0.12	0.34	0.30	0.11	0.12
Doxo	**	**	**	<0.09	**	<0.11	<0.49	<0.17	<0.81

GI_{50}: concentration that inhibits 50% cell growth or cytostatic effect after 48h-exposition. Tumor human cell lines: U251 = glioma, UACC-62 = melanoma; MCF-7 = breast; NCI-ADR/RES = multidrug resistant ovarian; NCI-H460 = lung, non-small cells; PC-3 = prostate; OVCAR-03 = ovarian; HT-29 = colon; K562 = leukemia; Non-tumor human line: HaCat = immortal keratinocyte; Doxo = Doxorubicin.

* The values of GI_{50} were not reached in the concentrations tested.

** SI values could not be calculated as $GI_{50\ (HaCat)}$ and $GI_{50\ (cancer\ cell\ lines)}$ are lower than 0.05 μmol·L^{-1}.

Considering the ovarian cancer cell line (OVCAR-03), PdHIB has shown a SI equal to 14.97, which is higher than that of doxorubicin (SI ≤ 0.49), K_2PdCl_4 (SI = 7.30) and K_2PtCl_4 (SI = 0.30). Although the activity of $[PdCl_2(HIB)_2]$ was lower than doxorubicin, its selectivity towards cancer cells was noticeable. The activity observed against OVCAR-3 is particularly interesting once this cell line is used as a model for cisplatin resistance in ovarian cancer [70,71]. In addition, HIB showed low activity against the cell lines tested, but its SI was higher than 1.0 for the cancer cell lines UACC-62 (melanoma), MCF-7 (breast), OVCAR-03 (ovarian) and K562 (leukemia).

When discussing the pharmacological potential of a molecule, we have to consider that each drug has a therapeutic window, or safety window, which is the range of concentration (dosage) that provides the desired efficiency with acceptable side effects. Specially in the case of cancer chemotherapy, the side effects are more acceptable due to the aggressive nature of the disease. That is why chemotherapy with cisplatin or doxorubicin are so aggressive, showing several side effects and considerably weakening the patient's health. However, such drugs are able to treat cancer with high efficiency.

The SI is a parameter that merely is related to the therapeutic window, therefore should be interpreted carefully. Hypothetically, the effective dosage of PdHIB to treat a patient with ovarian cancer would be much higher than doxorubicin or cisplatin, Nevertheless, a high dose of the complex would not be toxic and most of the side effects could be avoided.

4.9 Biophysical studies: interaction with DNA

The interactions between bio-macromolecules and pharmacological agents have attracted special interest among both chemistry and biology researchers during the past few decades.[72] Given that DNA is an important target for cisplatin and many metal complexes, the interaction between them have been studied extensively [73–77]. Damage caused by anticancer agents in the DNA of cancer cells may block their division and lead to cell death[78]. The interaction with DNA may occur in various ways including covalent binding and non-covalent modes such as intercalation, groove binding and electrostatic interaction. To investigate the presence of these interactions, several techniques are available, including UV spectrophotometry, circular dichroism spectroscopy and fluorescence studies with DNA intercalators [79–83].

4.9.1 Fluorescence studies with SYBR Green (SG)

SYBR Green (Figure 22) is a specific fluorophore that effectively interacts with double strand DNA, more specifically in the DNA minor groove[84], increasing its fluorescence emission upon complex formation by >1,000-fold[85].

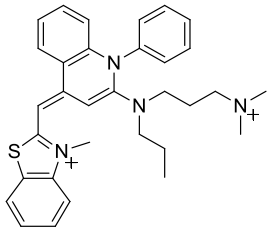

Figure 22. Molecular structure of SYBR Green.

It is possible to study the interaction of a compound with DNA by observing the reduction of the fluorescence emission intensity of SG due to competition and/or blocking of interaction by the molecule of interest.

As already presented, CT-DNA was incubated for 24 h at 37°C with HIB, PdHIB and PtHIB in the ratios (compound/DNA) of 0.1, 0.2 and 0.3. For each sample the fluorescence at 520 nm (maximum of SG) was monitored with the consecutive addition of SG (4μL of SG 10x). The results are shown in Figure 23. The fluorescence is presented relatively to the maximum intensity obtained for the free DNA in the presence of SG. It was necessary to normalize the errors due to experiments done in different days. The fluorescence of SG alone was measured and it is insignificant, thus not reported.

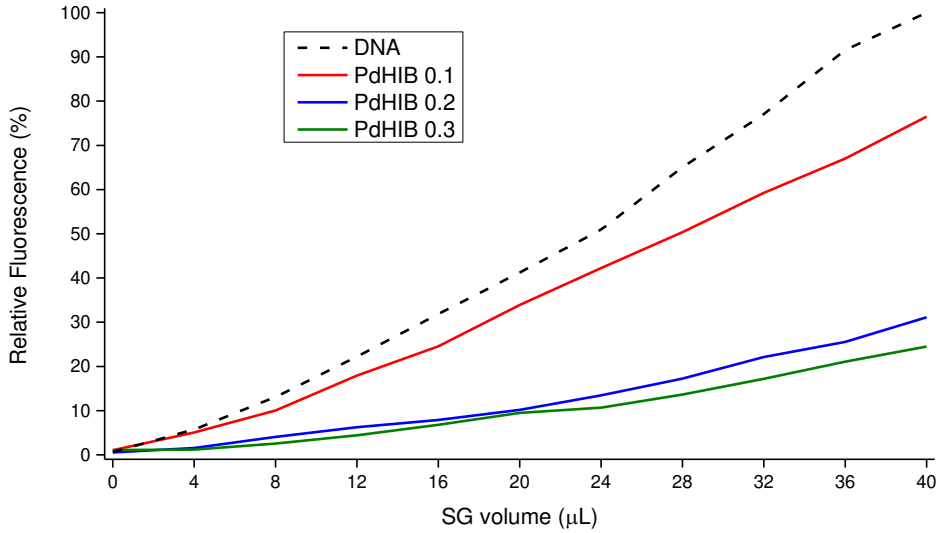

Figure 23. Relative fluorescence intensities of SG at 250 nm for samples of free DNA and DNA in the presence of PdHIB in the ratios (compound/DNA) 0.1, 0.2, 0.3.

For the samples of DNA incubated with HIB and PtHIB no significant fluorescence suppression is observed for all the concentrations tested. However, the samples of DNA incubated with PdHIB have a different profile. For the ratios of 0.2 and 0.3 the fluorescence intensity was decreased significantly suggesting interactions with DNA for ratios higher than 0.1, which seems to partially blocks SG interaction. The fluorescence suppression observed for this experiment may be a result of intercalation of PdHIB between the DNA bases or interaction with the DNA groove.

4.9.2 Circular dichroism spectroscopy

Circular dichroism spectroscopy is widely used to monitor conformational polymorphism of DNA, among many other aplications[82,83]. This technique is not able to provide information of molecules interacting with DNA at atomic level, for this reason, CD spectroscopy is primarily used empirically in studies with DNA. It is possible to differentiate DNA conformational changes between B-form, A-form, Z-form and other structures due to interactions with different compounds. The CT-DNA is characteristically a B-form right-handed DNA as shows the CD spectrum (Figure 24), where there is a positive band at 275 nm due to base stacking and negative band at 245 nm attributed to helicity[82,86]. In addition,

a positive band at 220 nm is also observed[83,87]. It was observed that HIB and PtHIB did not induce any noticeable changes in the CD spectrum even in the highest ratio tested.

The PdHIB complex, on the other hand, seems to alter the DNA conformation in the ratios 0.2 and 0.3 (Compound/DNA). In Figure 24, a comparison between the CD spectrum of CT-DNA in the absence and presence of PdHIB is presented.

For RI=0.1 it is observed a decrease in the intensity of all the bands and a slightly bathochromic shift, but the spectrum is still characteristic of a B-form DNA. However, for RI= 0.2 and RI=0.3 the CT-DNA suffers a significant destabilization of the B-form. The band intensities decreased and there is a great shift in the band at 275 nm suggesting alteration of the staking probably due to intercalation or covalent binding. Furthermore, the changes in the band at 245 nm indicate that the complex modify the helicity of DNA[73].

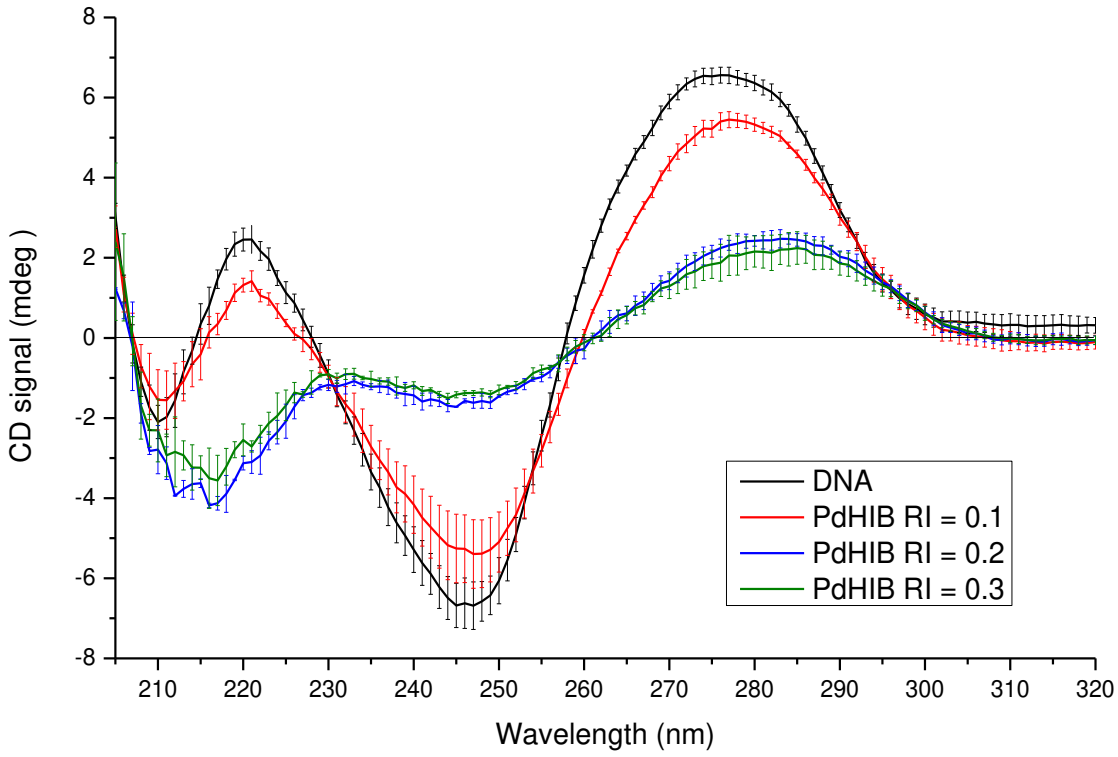

Figure 24. CD spectra of CT-DNA in absence and presence of PdHIB in the ratios (complex/ DNA) of 0.1, 0.2 and 0.3. The vertical bars represent the experimental error between three measurements.

5. Conclusions

Pd(II) and Pt(II) complexes with HIB were obtained with the coordination formulas $[PdCl_2(C_{13}H_{20}N_2O)_2]$ and $[PtCl_2(C_{13}H_{20}N_2O)_2]$ (1:2:2 metal/ ligand/ chloride). The compounds were characterized by mass spectrometry, and infrared and nuclear magnetic resonance spectroscopies. It was observed that the coordination of the ligand to the metal ions occurs by the nitrogen of the NH_2 group in a *trans* geometry. The structure of the PdHIB complex was solved by single-crystal X-ray diffraction studies.

Crystals suitable for X-ray diffraction were not obtained for PtHIB, however, its structural formula was suggested considering the spectroscopic data and DFT calculations. The DFT optimized structures of PdHIB and PtHIB were compared with the crystal structure of PdHIB and other similar crystals reported in the literature. It was shown that, not only the bond lengths and angles of the optimized structures were in accordance with the expected ones considering the crystal structure of the Pd(II) complex and others from the literature, but also that the functional PBE0 predicts this kind of coordination mode more appropriately than the B3LYP functional, which is frequently used by other authors.

The HIB was evaluated concerning its antibacterial and antiproliferative activities.[88] The MIC assay of HIB showed its *in vitro* activity against strains *S. aureus* (ATCC 25923) and *E. coli* (ATCC 25922) in the concentrations of 1850 $\mu g \cdot mL^{-1}$ and 3750 $\mu g \cdot mL^{-1}$, respectively. HIB also showed *in vitro* antiproliferative activity against six cancer cell lines in the micro molar range (92.14 – 511.10 $\mu mol \cdot L^{-1}$). It is interesting to notice that ibuprofen does not have antiproliferative or antibacterial properties, therefore the derivatization of ibuprofen to a hydrazide (HIB) was able to change some of its biological properties. The presence of free $NHNH_2$ moiety seems to be determinant for the activity of the compound.

On the other hand, the complexes were not active against the considered bacterial strains in the concentrations tested, and only PdHIB showed noticeable *in vitro* antiproliferative activity against ovarian cancer cell line (OVCAR-03) with GI_{50} 27.02 $\mu mol \cdot L^{-1}$. Interestingly, the PdHIB estimated selectivity index (SI) for OVCAR-03 was the higher observed in the experiment (TI > 14.97). This is because PdHIB inhibited the growth of the non-tumor cell line HaCat in a considerable higher concentration (GI_{50} > 404.6 $\mu mol \cdot L^{-1}$), which is an indication that the complex would be potentially safer to be administered *in vivo*. The low toxicity of PdHIB against normal cell lines is interesting as the systematic toxicity of

metal based drugs is currently a challenge in the medical clinic. Further preclinical and *in vivo* assays are needed to validate such hypothesis.

The overall low activities observed in the antiproliferative assays of the complexes may be attributed to the low solubility in the culture medium, even though low solubility of a metal complex is not necessarily a case of concern. For example, cisplatin is very insoluble in water, however it is administrated in a solution containing NaCl, NaOH and HCl in H_2O to assure a better solubility. The PdHIB complex could be further studied, for example, in a nano encapsulated formulation that would provide higher solubility and increased distribution in biological medium to evaluate the increase or decrease of activity and selectivity towards cancer cells.

The ligand and the respective complexes were evaluated concerning their interaction with CT-DNA. Only PdHIB showed a considerable interaction with DNA, by intercalation or covalent bond, causing structural changes as evidenced by CD spectroscopy. This interaction was also indicated by fluorescence studies of competitive interaction to DNA using SG probe, as the fluorescence intensity of SG with CT-DNA was decreased by the presence of PdHIB. This suggests that the higher antiproliferative activity of PdHIB in comparison to PtHIB is due to the former's capacity of interaction with DNA, which is the main target for this kind of metallodrugs. The interaction of PdHIB (and not PtHIB) with DNA could be explained by the differences on reactivity between the Pd(II) and the analogous Pt(II) complexes, as Pd(II) complexes usually have faster reaction kinetics and could react with DNA promptly. Also, the lower solubility of PtHIB could have hampered its interaction with the DNA, as the complex availability in solution is inferior.

6. Bibliographic references

1. Hanahan, D. & Weinberg, R. A. The hallmarks of cancer. *Cell* **100,** 57–70 (2000).
2. Yang, E. J., Wu, C., Liu, Y., Lv, J. & Sup Shim, J. Revisiting Non-Cancer Drugs for Cancer Therapy. *Curr. Top. Med. Chem.* **16,** 2144–2155 (2016).
3. Biemar, F. & Foti, M. Global progress against cancer-challenges and opportunities. *Cancer Biol. Med.* **10,** 183–186 (2013).
4. Zugazagoitia, J. *et al.* Current Challenges in Cancer Treatment. *Clin. Ther.* **38,** 1551–1566 (2016).
5. Rosenberg, B., Van Camp, L. & Krigas, T. Inhibition of Cell Division in Escherichia coli by Electrolysis Products from a Platinum Electrode. *Nature* **205,** 698–699 (1965).
6. Rosenberg, B., Van Camp, L., Trosko, J. & Mansour, V. Platinum Compounds: a New Class of Potent Antitumour Agents. *Nature* **222,** 385–386 (1969).
7. Medici, S. *et al.* Noble metals in medicine: Latest advances. *Coord. Chem. Rev.* **284,** 329–350 (2015).
8. Wheate, N. J., Walker, S., Craig, G. E. & Oun, R. The status of platinum anticancer drugs in the clinic and in clinical trials. *Dalt. Trans.* **39,** 8113–8127 (2010).
9. Pinato, O., Musetti, C. & Sissi, C. Pt-based drugs: the spotlight will be on proteins. *Metallomics* **6,** 380–395 (2014).
10. Ramachandran, S., Quist, A. P., Kumar, S. & Lal, R. Cisplatin Nanoliposomes for Cancer Therapy: AFM and Fluorescence Imaging of Cisplatin Encapsulation, Stability, Cellular Uptake, and Toxicity. *Langmuir* **22,** 8156–8162 (2006).
11. Wang, X., Wang, X. & Guo, Z. Functionalization of Platinum Complexes for Biomedical Applications. *Acc. Chem. Res.* **48,** 2622–2631 (2015).
12. Apps, M. G., Choi, E. H. Y. & Wheate, N. J. The state-of-play and future of platinum drugs. *Endocr. Relat. Cancer* **22,** R219–R233 (2015).
13. Neidle, S., Ismail, I. M. & Sadler, P. J. The structure of the antitumor complex cis-(diammino) (1,1-cyclobutanedicarboxylato)-Pt(II): X ray and NMR studies. *J. Inorg. Biochem.* **13,** 205–212 (1980).
14. Frey, U., Ranford, J. D. & Sadler, P. J. Ring-Opening Reactions of the Anticancer Drug Carboplatin: NMR Characterization of cis-[Pt(NH3)2(CBDCA-O)(5′-GMP-N7)] in Solution. *Inorg. Chem.* **32,** 1333–1340 (1993).
15. Kasparkova, J., Vojtiskova, M., Natile, G. & Brabec, V. Unique properties of DNA interstrand cross-links of antitumor oxaliplatin and the effect of chirality of the carrier ligand. *Chem. - A Eur. J.* **14,** 1330–1341 (2008).
16. Coluccia, M. & Natile, G. Trans-Platinum Complexes in Cancer Therapy. *Anticancer. Agents*

Med. Chem. **7,** 111–123 (2007).

17. Peterson, E. J. *et al.* Antiangiogenic platinum through glycan targeting. *Chem. Sci.* **8,** 241–252 (2017).
18. Farrell, N. P. Multi-platinum anti-cancer agents. Substitution-inert compounds for tumor selectivity and new targets. *Chem. Soc. Rev.* **44,** 8773–8785 (2015).
19. Qu, Y., Kipping, R. G. & Farrell, N. P. Solution studies on DNA interactions of substitution-inert platinum complexes mediated via the phosphate clamp. *Dalt. Trans.* **44,** 3563–3572 (2015).
20. de Souza, G. D. *et al.* A New Complex of Palladium(II) With 2-Furoic Hydrazide: Synthesis, Characterization, Theoretical Calculations and Biological Studies. *Croat. Chem. Acta* **86,** 201–206 (2013).
21. Garoufis, A., Hadjikakou, S. K. & Hadjiliadis, N. Palladium coordination compounds as anti-viral, anti-fungal, anti-microbial and anti-tumor agents. *Coord. Chem. Rev.* **253,** 1384–1397 (2009).
22. Harris, R. E., Beebe-Donk, J., Doss, H. & Burr Doss, D. Aspirin, ibuprofen, and other non-steroidal anti-inflammatory drugs in cancer prevention: a critical review of non-selective COX-2 blockade. *Oncol. Rep.* **13,** 559–583 (2005).
23. Rayburn, E. R., Ezell, S. J. & Zhang, R. Anti-Inflammatory Agents for Cancer Therapy. *Mol. Cell* **1,** 29–43 (2009).
24. Baron, J. A. & Sandler, R. S. Nonsteroidal Anti-Inflammatory drugs and Cancer Prevention. *Annu. Rev. Med.* **51,** 511–523 (2000).
25. Qu, X. *et al.* Hydrolysis of ibuprofenoyl-CoA and other 2-APA-CoA esters by human acyl-CoA thioesterases-1 and -2 and their possible role in the chiral inversion of profens. *Biochem. Pharmacol.* **86,** 1621–1625 (2013).
26. Lloyd, M. D. *et al.* a-Methylacyl-CoA racemase (AMACR): Metabolic enzyme, drug metabolizer and cancer marker P504S. *Prog. Lipid Res.* **52,** 220–230 (2013).
27. Park, S.-S. *et al.* P504S expressing circulating prostate cells as a marker for prostate cancer. *Oncol. Rep.* **24,** 687–692 (2010).
28. Evans, A. J. Alpha-methylacyl CoA racemase (P504S): overview and potential uses in diagnostic pathology as applied to prostate needle biopsies. *J. Clin. Pathol.* **56,** 892–897 (2003).
29. Kokki, H. Nonsteroidal anti-inflammatory drugs for postoperative pain: a focus on children. *Paediatr. Drugs* **5,** 103–123 (2003).
30. Pereira E Silva, I. M. *et al.* A silver complex with ibuprofen: Synthesis, solid state characterization, DFT calculations and antibacterial assays. *J. Mol. Struct.* **1049,** 1–6 (2013).
31. Fiori, A. T. M., Lustri, W. R., Magalhães, A. & Corbi, P. P. Chemical, spectroscopic characterization and antibacterial activities in vitro of a novel gold(I)-ibuprofen complex. *Inorg.*

Chem. Commun. **14,** 738–740 (2011).

32. Dendrinou-Samara, C. *et al.* Anti-inflammatory drugs interacting with Zn(II), Cd(II) and Pt(II) metal ions. *J. Inorg. Biochem.* **71,** 171–179 (1998).
33. Trinchero, A., Bonora, S., Tinti, A. & Fini, G. Spectroscopic Behavior of Copper Complexes of Nonsteroidal Anti-Inflammatory Drugs. *Biopolymers* **74,** 120–124 (2004).
34. Lay, P. & Hambley, T. Prophylaxis or treatment of cardiovascular inflammation. (2007). <https://encrypted.google.com/patents/WO2007110755A1?cl=ko> Accessed: 13/03/2018.
35. Bakhtiar, R. & Ochiai, E. I. Pharmacological applications of inorganic complexes. *Gen. Pharmacol.* **32,** 525–540 (1999).
36. Kansara, S. G., Pandit, R. D. & Bhawe, V. G. Synthesis of some new Ibuprofen derivatives containing chief heterocyclic moiety like s-Triazine and evaluated for their analgesic activity. *Rasayan J. Chem.* **2,** 699–705 (2009).
37. Li, Y.-R. *et al.* Synthesis and biological evaluation of 1,3-diaryl pyrazole derivatives as potential antibacterial and anti-inflammatory agents. *Bioorg. Med. Chem. Lett.* **25,** 5052–5057 (2015).
38. Zawidlak-Wegrzynska, B. *et al.* Synthesis and antiproliferative properties of ibuprofen-oligo(3-hydroxybutyrate) conjugates. *Eur. J. Med. Chem.* **45,** 1833–1842 (2010).
39. Amir, M. & Kumar, S. Synthesis and evaluation of anti-inflammatory, analgesic, ulcerogenic and lipid peroxidation properties of ibuprofen derivatives. *Acta Pharm.* **57,** 31–45 (2007).
40. Reddy, L. V. *et al.* Design and synthesis of 1-aroyl-2-ylidene hydrazines under conventional and microwave irradiation conditions and their cytotoxic activities. *J. Braz. Chem. Soc.* **21,** 98–104 (2010).
41. Kumar, P. & Narasimhan, B. Hydrazides/ Hydrazones as Antimicrobial and Anticancer Agents in the New Millennium. *Mini-Reviews Med. Chem.* **13,** 971–987 (2013).
42. Poggi, M. *et al.* New Isoniazid Complexes, Promising Agents Against Mycobacterium tuberculosis. *J. Mex. Chem. Soc.* **57,** 198–204 (2013).
43. West, E. D. & Dally, P. J. Effects of Iproniazid in Depressive Syndromes. *Br. Med. J.* **1,** 1491–1494 (1959).
44. Finch, R. A., Shyam, K., Penketh, P. G. & Sartorelli, A. C. 1,2-Bis(methylsulfonyl)-1-(2-chloroethyl)-2-(methylamino)carbonylhydrazine (101M): A Novel Sulfonylhydrazine Prodrug with Broad-Spectrum Antineoplastic Activity. *Cancer Res.* **61,** 3033–3038 (2001).
45. Pearson, R. G. Hard and Soft Acids and Bases. *J. Am. Chem. Soc.* **85,** 3533–3539 (1963).
46. Adamo, C. & Barone, V. Toward reliable density functional methods without adjustable parameters: The PBE0 model. *J. Chem. Phys.* **110,** 6158–6170 (1999).
47. Eichkorn, K., Weigend, F., Treutler, O. & Ahlrichs, R. Auxiliary basis sets for main row atoms and transition metals and their use to approximate Coulomb potentials. *Theor. Chem. Acc.* **97,** 119–124 (1997).

48. Neese, F. The ORCA program system. *Wiley Interdiscip. Rev. Comput. Mol. Sci.* **2,** 73–78 (2012).
49. Izsák, R. & Neese, F. An overlap fitted chain of spheres exchange method. *J. Chem. Phys.* **135,** 144105 (2011).
50. CLSI. *Performance Standards for Antimicrobial Susceptibility Testing; Twenty-Third Informational Supplement (CLSI Document M100-S23)*. *Clinical and Laboratory Standards Institute* **33,** (2013).
51. Nunes, J. H. B. *et al.* Synthesis, characterization and in vitro biological assays of a silver(I) complex with 5-fluorouracil: a strategy to overcome multidrug resistant tumor cells. *J. Fluor. Chem.* **195,** 93–101 (2017).
52. Bachiega, P. *et al.* Antioxidant and antiproliferative activities in different maturation stages of broccoli (Brassica oleracea Italica) biofortified with selenium. *Food Chem.* **190,** 771–776 (2016).
53. de Almeida, M. S. *et al.* Synthesis, DNA Binding, and Antiproliferative Activity of Novel Acridine-Thiosemicarbazone Derivatives. *Int. J. Mol. Sci.* **16,** 13023–13042 (2015).
54. Marchetti, G. M. *et al.* The anticancer activity of dichloromethane crude extract obtained from Calea pinnatifida. *J. Exp. Pharmacol.* **4,** 157–162 (2012).
55. Monks, A. *et al.* Feasibility of a High-Flux Anticancer Drug Screen Using a Diverse Panel of Cultured Human Tumor Cell Lines. *JNCI J. Natl. Cancer Inst.* **83,** 757–766 (1991).
56. Nakka, M. *et al.* Naproxen and ibuprofen based acyl hydrazone derivatives: Synthesis, structure analysis and cytotoxicity studies. *J. Chem. Pharm. Res.* **2,** 393–409 (2010).
57. Carvalho, M. a *et al.* Synthesis, spectroscopic characterization, DFT studies, and initial antibacterial assays in vitro of a new palladium(II) complex with tryptophan. *J. Coord. Chem.* **65,** 1700–1711 (2012).
58. Carvalho, M. A. *et al.* Chemical and spectroscopic characterizations, ESI-QTOF mass spectrometric measurements and DFT studies of new complexes of palladium(II) with tryptamine and mefenamic acid. *J. Mol. Struct.* **1100,** 6–13 (2015).
59. Spera, M. B. M. *et al.* Palladium(II) complex with S-allyl-l-cysteine: New solid-state NMR spectroscopic measurements, molecular modeling and antibacterial assays. *Spectrochim. Acta - Part A Mol. Biomol. Spectrosc.* **78,** 313–318 (2011).
60. Abbehausen, C. *et al.* Synthesis, spectroscopic characterization, DFT studies, and antibacterial and antitumor activities of a novel water soluble Pd(II) complex with l-alliin. *J. Mol. Struct.* **1035,** 421–426 (2013).
61. Sousa, L. M. *et al.* Spectroscopic characterization and molecular modeling of novel palladium(II) complexes with carbazates and hydrazides. *J. Mol. Struct.* **1097,** 15–22 (2015).
62. Carvalho, M. A. *et al.* A new platinum complex with tryptophan: Synthesis, structural characterization, DFT studies and biological assays in vitro over human tumorigenic cells.

Spectrochim. Acta - Part A Mol. Biomol. Spectrosc. **122,** 209–215 (2014).

63. Rodrigues, M. A. *et al.* Platinum(II) complexes with carbazates and hydrazides: Synthesis, spectral characterization, computational modeling, and biological studies. *Polyhedron* **98,** 146–153 (2015).
64. Drozdzewski, P., Brozyna, A., Kubiak, M. & Lis, T. Synthesis, structure and vibrational spectroscopy of palladium (II) complexes with 2-thiophenecarboxylic hydrazide (tch): Crystal structure of [PdCl2(tch)2]. 2dmf. *Vib. Spectrosc.* **40,** 118–126 (2006).
65. Nakamoto, K. *Infrared and Raman Spectra of Inorganic and Coordination Compounds - Part B: Application in Coordination, Organometallic and Bioinorganic Chemistry*. (John Wiley & Sons, 2009).
66. Silverstein, M. R., Webster, F. X. & Kiemle, D. J. *Spectrometric Identification of Organic Compounds*. (John Wiley & Sons, 2005). doi:10.1016/0022-2860(76)87024-X
67. Alvarez-Larena, A., Piniella, J. F., Borrell, J. I. & Beti, C. Crystal structure of dichloro(1,6-diaminotetrahydropyrrolo[2,3-b]pyrrole-2,5(1H,4H)-dione)platinum(II),Pt(C6H10N4O2)Cl2. *Zeitschrift für Kristallographie - Crystalline Materials* **209,** 293 (1994).
68. Tacar, O., Sriamornsak, P. & Dass, C. R. Doxorubicin: An update on anticancer molecular action, toxicity and novel drug delivery systems. *J. Pharm. Pharmacol.* **65,** 157–170 (2013).
69. Muller, P. Y. & Milton, M. N. The determination and interpretation of the therapeutic index in drug development. *Nat. Rev. Drug Discov.* **11,** 751–761 (2012).
70. Sakhare, S. S., Rao, G. G., Mandape, S. N. & Pratap, S. Transcriptome profile of OVCAR3 cisplatin-resistant ovarian cancer cell line. *BMC Bioinformatics* **15,** P21 (2014).
71. Hamilton, T. C. *et al.* Characterization of a Human Ovarian Carcinoma Cell Line (NIH:OVCAR-3) with Androgen and Estrogen Receptors. *Cancer Res.* **43,** 5379–5389 (1983).
72. Krishnamoorthy, P. *et al.* Copper(I) and nickel(II) complexes with 1:1 vs. 1:2 coordination of ferrocenyl hydrazone ligands: Do the geometry and composition of complexes affect DNA binding/cleavage, protein binding, antioxidant and cytotoxic activities? *Dalt. Trans.* **41,** 4423–4436 (2012).
73. Zanvettor, N. T. *et al.* Inorganica Chimica Acta Copper (II), palladium (II) and platinum (II) complexes with 2,2-thiophen-yl-imidazole: Synthesis, spectroscopic characterization, X-ray crystallographic studies and interactions with calf-thymus DNA. *Inorg. Chim. Acta* **443,** 304–315 (2016).
74. Tan, C., Liu, J., Chen, L., Shi, S. & Ji, L. Synthesis, structural characteristics, DNA binding properties and cytotoxicity studies of a series of Ru(III) complexes. *J. Inorg. Biochem.* **102,** 1644–1653 (2008).
75. Shahabadi, N., Mohammadi, S. & Alizadeh, R. DNA interaction studies of a new platinum(II) complex containing different aromatic dinitrogen ligands. *Bioinorg. Chem. Appl.* **2011,** 1–8 (2011).

76. Shahabadi, N. & Mohammadi, S. Synthesis characterization and DNA interaction studies of a new Zn(II) complex containing different dinitrogen aromatic ligands. *Bioinorg. Chem. Appl.* **2012,** 1–8 (2012).
77. Ljubijankić, N., Zahirović, A., Turkušić, E. & Kahrović, E. DNA Binding Properties of Two Ruthenium(III) Complexes Containing Schiff Bases Derived from Salicylaldehyde: Spectroscopic and Electrochemical Evidence of CT DNA Intercalation. *Croat. Chem. Acta* **86,** 215–222 (2013).
78. Jung, Y. & Lippard, S. J. Direct cellular responses to platinum-induced DNA damage. *Chem. Rev.* **107,** 1387–1407 (2007).
79. Sirajuddin, M., Ali, S. & Badshah, A. Drug-DNA interactions and their study by UV-Visible , fluorescence spectroscopies and cyclic voltametry. *J. Photochem. Photobiol. B Biol.* **124,** 1–19 (2013).
80. Kyros, L. *et al.* Synthesis, characterization, and binding properties towards CT-DNA and lipoxygenase of mixed-ligand silver(I) complexes with 2-mercaptothiazole and its derivatives and triphenylphosphine. *J. Biol. Inorg. Chem.* **19,** 449–464 (2014).
81. Zaki, M., Arjmand, F. & Tabassum, S. Current and future potential of metallo drugs: Revisiting DNA-binding of metal containing molecules and their diverse mechanism of action. *Inorganica Chim. Acta* **444,** 1–22 (2016).
82. Kypr, J., Kejnovská, I., Renčiuk, D. & Vorlíčková, M. Circular dichroism and conformational polymorphism of DNA. *Nucleic Acids Res.* **37,** 1713–1725 (2009).
83. Chang, Y.-M., Chen, C. K.-M. & Hou, M.-H. Conformational changes in DNA upon ligand binding monitored by circular dichroism. *Int. J. Mol. Sci.* **13,** 3394–413 (2012).
84. Dragan, A. I. *et al.* SYBR Green I: Fluorescence properties and interaction with DNA. *J. Fluoresc.* **22,** 1189–1199 (2012).
85. Zipper, H., Brunner, H., Bernhagen, J. & Vitzthum, F. Investigations on DNA intercalation and surface binding by SYBR Green I, its structure determination and methodological implications. *Nucleic Acids Res.* **32,** 1–10 (2004).
86. Loganathan, R. *et al.* Mixed ligand copper(II) complexes of N,N-bis(benzimidazol-2-ylmethyl)amine (BBA) with diimine co-ligands: efficient chemical nuclease and protease activities and cytotoxicity. *Inorg. Chem.* **51,** 5512–5532 (2012).
87. Zabost, E., Nowicka, A. M., Donten, M. & Stojek, Z. Substantial difference between temperature dependencies of dsDNA predenaturation process obtained by voltammetry and spectroscopy. *Phys. Chem. Chem. Phys.* **11,** 8933–8938 (2009).
88. Manzano, C. M. *et al.* Pt(II) and Pd(II) complexes with ibuprofen hydrazide: Characterization, theoretical calculations, antibacterial and antitumor assays and studies of interaction with CT-DNA. *J. Mol. Struct.* **1154,** 469–479 (2018).

7. Appendix

Table S1 – Crystallographic experimental details.

Chemical formula	$PdC_{26}H_{40}N_4O_2Cl_2$
M.W. ($gmol^{-1}$)	617.92
Crystal system	Monoclinic
Space group	$P2_1/c$
Temperature (K)	150
a, b, c (Å)	27.8148 (5), 8.9319 (3), 11.5187 (3)
β (°)	92.462 (2)
V ($Å^3$)	2859.05 (13)
Z	4
Radiation type	[Mo] Kα
μ (mm^{-1})	0.87
Crystal size (mm)	0.27 × 0.11 × 0.05
Diffractometer	Bruker APEX-II CCD
Absorption correction	Multi-scan, CrysAlis PRO 1.171.38.41 (Rigaku Oxford Diffraction, 2015) Empirical absorption correction using spherical harmonics, implemented in SCALE3 ABSPACK scaling algorithm.
T_{min}, T_{max}	0.974, 1.000
Number of measured, independent and observed *[I > 2σ(I)]* reflections	43664, 5855, 5262
R_{int}	0.037
$(\sin \theta/\lambda)_{max}$ ($Å^{-1}$)	0.625

$R[F^2 > 2\sigma(F^2)]$, $wR(F^2)$, S	0.043, 0.103, 1.05
Number of reflections	5855
Number of parameters	361
Number of restraints	72
H-atom treatment	H-atoms parameters constrained, $w = 1/[\sigma^2(F_o^2) + (0.0417P)^2 + 10.0059P]$ where $P = (F_o^2 + 2F_c^2)/3$
Δρmax, Δρmin (e Å^{-3})	1.92, −1.19

Table S2 - Bond lengths of $[PdCl_2(HIB)_2]$ and a similar Pd(II) complex reported in the literature.

Atoms	**Bond length (Å) $[PdCl_2(HIB)_2]$**	**Bond length (Å) literature***
Pd-Cl1/Pd-Cl2	2.309(1)/2.2889(9)	2.303
Pd-N1B/Pd-N1A	2.048(3)/2.036(3)	2.052
N1A-N2A/N1B-N2B	1.425(4)/1.408(4)	1.431(5)
C1B-O1B/C1A-O1A	1.226(5)/1.224(4)	1.236(5)

* P. Drozdzewski, A. Brozyna, M. Kubiak, T. Lis, Vib. Spectrosc. 40 (2006) 118–126.

Table S3 - Angles and torsions of $[PdCl_2(HIB)_2]$ and a similar Pd(II) complex reported in the literature.

Atoms	**Angles/torsions (°) $[PdCl_2(HIB)_2]$**	**Angles/torsions (°) literature***
Cl2-Pd-Cl1	177.41(4)	180.0
N1B-Pd-N1A	178.6(1)	180.0
N2A-N1A-Pd/N2B-N1B-Pd	113.1(2)/112.6(2)	114.6/114.6
O1B-C1B-N2B/O1A-C1A-N2A	121.5(4)/121.4(3)	122.7(4)/122.7(4)
C1B-N2B-N1B/C1A-N2A-N1A	118.9(3)/116.8(3)	116.6(3)/116.6(3)

C1B-N2B-N1B-Pd/ C1A-N2A-N1A-Pd	119.6(3)/ -109.8(3)	114.2/114.2
N2B-N1B-Pd-Cl1/ N2A-N1A-Pd-Cl2	68.7(2)/ -69.0(2)	63.9/-63.9
N2B-N1B-Pd-Cl2/ N2A-N1A-Pd-Cl1	-113.5(2)/ 108.8(2)	116.1/-116.1

* P. Drozdzewski, A. Brozyna, M. Kubiak, T. Lis, Vib. Spectrosc. 40 (2006) 118–126.

Table S4 - Bond lengths for the HIB molecules in PdHIB crystal and those found for 188 ibuprofen/ibuprofenate entries on CSD.

Atoms	**Mean bond lengths (Å) found on CSD**	**Bond lengths (Å) for HIB in PdHIB crystal***
C3-C4	1.383(2)	1.390(6)/1.384(6)
C4-C5	1.387(2)	1.392(6)/1.386(6)
C5-C8	1.387(2)	1.370(6)/1.379(7)
C7-C8	1.385(2)	1.368(6)/1.377(6)
C6-C7	1.382(2)	1.356(7)/1.395(6)
C8-C9	1.514(3)	1.52(2) [1.533(7)]/ 1.514(7)
C3-C6	1.384(2)	1.383(6)/ 1.385(6)
C2-C3	1.519(3)	1.525(6)/ 1.514(5)
C1-C2	1.521(2)	1.539(6)/ 1.525(5)
C2-C13	1.520(3)	1.507(7)/ 1.540(5)
C1-O1	1.257(5)	1.226(5)/ 1.224(4)
C9-C10	1.513(4)	1.61(2) [1.562(9)]/ 1.536(8)
C10-C12	1.507(7)	1.43(3) [1.47(1)]/ 1.527(9)
C10-C11	1.510(5)	1.49(3) [1.50(1)]/ 1.47(1)

*the values in braces corresponds to the bond lengths of the disordered groups with lower level of occupation.

Table S5 - Angles for the HIB molecules and those found for 188 ibuprofen/ibuprofenate entries on CSD.

Atoms	Mean angles (°) found on CSD	Angles (°) for HIB in PdHIB crystal*
C3-C4-C5	120.7(1)	120.2(4)
C4-C5-C8	121.4(2)	121.6(4)
C4-C3-C6	117.9(1)	118.1(4)
C2-C3-C4	120.7(3)	122.1(4)
C5-C8-C7	117.4(2)	117.8(4)
C5-C8-C9	121.2(2)	121.5(4)
C7-C8-C9	121.4(2)	120.6(4)
C6-C7-C8	121.3(1)	121.2(4)
C8-C9-C10	114.2(2)	113.9(5)
C3-C6-C7	121.2(1)	121.0(4)
C6-C3-C2	121.3(4)	119.7(3)
C1-C2-C3	109.1(2)	111.4(3)
C3-C2-C13	112.7(3)	114.4(3)
C1-C2-C13	110.7(3)	106.5(3)
C2-C1-O1	118.2(5)	124.8(3)
C9-C10-C11	111.7(6)	110.0(5)
C9-C10-C12	111.2(5)	113.0(5)
C11-C10-C12	111.2(4)	110.5(6)

*the values in braces corresponds to the angles of the disordered groups with lower level of occupation.

Table S6 – Atomic coordinates of the DFT optimized structure of $[PdCl_2(HIB)_2]$

	x	y	Z
Pd	14.52299513997010	1.37780269510770	5.42146123680676
Cl	13.58700985026270	3.22129131213484	6.44007809022994
Cl	15.38331341831400	-0.52270205274187	4.43120658277483
O	18.38839241763340	3.43847816817575	5.33086034534251
O	11.85831170130270	1.49940416676350	2.33392296710987
N	16.34606416439610	1.95543289462689	6.17315080716588
N	17.46388433897110	1.39522937595500	5.52921300423203
H	17.20300490735910	0.56343160841211	5.00183205708294
N	12.75381770851890	0.74728053633405	4.63043371526504
N	11.65294617208750	1.61877835378209	4.56968631343219
H	11.68537302227820	2.31922619464788	5.30691272302085
C	18.35235326227820	2.27638910513652	4.97832864176385
C	19.18273289312290	1.66690707892809	3.86584559550423
H	19.26306207685060	0.59215673097152	4.06364162705525
C	18.39513256481490	1.83788851916112	2.57670716554661
C	17.76418228240560	3.04053757675336	2.27097792390243
H	17.82981461798690	3.87309457614410	2.96258383077229
C	17.03116139046790	3.17484460099108	1.10384350391240
H	16.52767769140420	4.11382135236590	0.89927406691102
C	16.91272793398240	2.12746109674582	0.19514932460988
C	17.54973138453270	0.92854690065727	0.50512943276649
H	17.45584113674870	0.08432081869979	-0.17125040107784
C	18.27073543740940	0.78232670400354	1.68053247976408
H	18.72905402448400	-0.17395776985284	1.91270569165288
C	16.13459664309820	2.28772984631669	-1.07936958158324
H	15.30533592390490	2.98500323958929	-0.91397059842636
H	15.68308087067490	1.32670185125970	-1.34644949309396
C	16.96549887504530	2.78818135302530	-2.27157258043458
H	17.83759752733240	2.12759074481315	-2.36082638275633
C	17.46218237963780	4.21187726620302	-2.06866418810818
H	16.61733093038870	4.90583048062966	-2.00427117885674
H	18.08460887963480	4.52905738451912	-2.90884512454634
H	18.05484371181790	4.31422311241406	-1.15771505757945
C	16.16114310010820	2.69198681887508	-3.56040502021242
H	15.82052771290520	1.67061956011550	-3.75198721987143
H	16.75831324033310	3.02071454513652	-4.41527499523208
H	15.27511322366250	3.33248379718539	-3.51131326723044
C	20.58538311854050	2.25337277342144	3.78625514785279

H	21.13480826867330	2.07502950508510	4.71366029550486
H	20.55067810112270	3.32791993629459	3.60310205940243
H	21.13144340904040	1.78167110778063	2.96827265221161
C	11.35194933863710	2.04116233307680	3.29383114273015
C	10.36380629581830	3.19089277066389	3.23150193405179
H	9.83597447116218	3.22045065732185	4.18976535938265
C	9.34304852353077	2.95445397857367	2.14599206072969
C	8.00509420605484	2.76772666254291	2.47013846259352
H	7.69274018695443	2.82347481293851	3.50904958008916
C	7.06381703931754	2.49215583808762	1.48904838499548
H	6.02780998817731	2.33462604505441	1.77379722295109
C	7.43519096069395	2.37862233878013	0.15331609703198
C	8.77481946286324	2.58599688333401	-0.16673941751178
H	9.09370987880931	2.49562492396982	-1.20028225716155
C	9.71407265434786	2.87695903826289	0.80637284740310
H	10.75212738782710	3.00363934001168	0.52570903245276
C	6.43439891818333	2.03008237192677	-0.90891355404156
H	5.67939975207412	1.36181618911503	-0.48250966417891
H	6.93856555015005	1.46365569621161	-1.70088209429541
C	5.71444826615956	3.21934060393624	-1.56349566218427
H	5.17543821512659	3.76151722158942	-0.77546629915427
C	6.68214525071831	4.18777113236809	-2.22680787259016
H	6.14156030682569	5.00223431515357	-2.71553717707338
H	7.27229362908563	3.67479515971463	-2.99441943632569
H	7.37702107791951	4.62710012331142	-1.50837472584784
C	4.69851938022977	2.69695132120105	-2.57043514209352
H	4.15560565701612	3.51304563975722	-3.05453102372979
H	3.96780057122875	2.03841911424211	-2.09277233371450
H	5.20253227759982	2.12232101509094	-3.35467201561531
C	11.13233408334060	4.50807892710105	3.07090975919179
H	10.42741883565970	5.34089139444716	3.09496977148540
H	11.66780238194050	4.53605767214049	2.12139619254721
H	11.85798470707840	4.64474173027949	3.87653853258707
H	16.37462556629780	1.72796631540731	7.16423967162922
H	16.45012068961280	2.97321083226826	6.09797534675064
H	12.47768995745760	-0.10538349625381	5.10991960707147
H	12.94707507859620	0.49951623180669	3.65033547725660

Table S7 - Atomic coordinates of the DFT optimized structure of $[PtCl_2(HIB)_2]$

	x	y	z
Pt	13.09671553565640	3.71628718190179	-0.11631684120704
Cl	12.64505876499310	5.88350921384581	0.52611561615750
Cl	13.48127388333970	1.52091553555151	-0.72928269122925
O	16.83907419162850	3.86450827788677	2.27720533492105
O	8.80794731323724	3.72796285878035	-1.72942605635114
N	15.05899473986270	4.08127357257898	0.36454784818861
N	15.93141238340050	2.97785177674945	0.42870088161498
H	15.53271688365740	2.14147260563934	0.01185303772234
N	11.15419862451150	3.34012777058258	-0.63157182365186
N	10.13209730986730	4.00393294636457	0.07085796822730
H	10.48931583821530	4.71928988519033	0.69354293051021
C	16.74579558808140	2.91550038479710	1.52287033485985
C	17.49570889787930	1.60814549835795	1.68509611843019
H	17.02332695433410	0.86759163411883	1.03136241533359
C	18.94688747483380	1.71625296641657	1.25918829629873
C	19.76032940664740	2.78031500329312	1.63496087198465
H	19.33453668655900	3.60580482747958	2.19465658372045
C	21.10646304791190	2.79486339889276	1.29484526967990
H	21.71565158046370	3.64308653086425	1.59108268715141
C	21.68796591142570	1.74751999763711	0.58338485335478
C	20.86454615055020	0.68852698345741	0.21007389172033
H	21.28348472502620	-0.13385250284476	-0.36123285983905
C	19.51791689449170	0.67430385521030	0.53446674424945
H	18.90062490751220	-0.15944756902967	0.21408086931420
C	23.14352727651940	1.73736836276878	0.20789420254400
H	23.48845356821120	2.76225738552943	0.02588858946637
H	23.25060329312580	1.19949567179406	-0.73926620822043
C	24.07675933954430	1.08036004238150	1.23800594067152
H	23.61913146608360	0.12824781648022	1.53561097679498
C	24.24650230907500	1.93365750052983	2.48667168795688
H	24.75666764844990	2.87111194490832	2.24074851679165
H	24.85121464269160	1.41423200837585	3.23427514086902
H	23.28827534986690	2.18495688790916	2.94728452471359
C	25.43158713836170	0.78287488230488	0.60566445961601
H	25.33769703735220	0.11449785620332	-0.25387768322517
H	26.10643947450140	0.31078889820836	1.32410561372803

H	25.90746259498410	1.70541579689168	0.25666741120799
C	17.38691434592500	1.12667231968517	3.13354238594096
H	16.34982216294230	0.91853951457613	3.40708228972470
H	17.77848345612410	1.88550628926777	3.81143487668953
H	17.97123531255590	0.21433453812758	3.26212810707801
C	8.96429664791337	4.20087630414510	-0.62242132962981
C	7.89751033110001	4.97207272408247	0.12640185086732
H	8.38546445276825	5.55816432474432	0.91141438143061
C	6.96372422280934	3.98892154358894	0.80844817313138
C	6.86701770338694	3.96590395386924	2.19614452652004
H	7.46628236432318	4.65272637088366	2.78596974835865
C	6.02055145331713	3.07721686187234	2.83836713613786
H	5.97532859459218	3.08088279905940	3.92305835786751
C	5.23515298811506	2.18070773843726	2.11687224108023
C	5.33876474411878	2.20594134634409	0.72871619062702
H	4.74738120068232	1.51135235444284	0.14016199105343
C	6.18723935313785	3.09138212793181	0.08049763434635
H	6.25804007097326	3.06683147066461	-1.00133282845714
C	4.30800148545929	1.23333672418644	2.82627043616053
H	4.86367235532967	0.71542867510188	3.61656809463893
H	3.96530743169651	0.45978770560511	2.13041769462300
C	3.08316948008489	1.91151524578389	3.45576105952914
H	3.44990536218447	2.74828335703245	4.06336472107727
C	2.14135703316970	2.46862298490905	2.39830281959026
H	1.31864771973710	3.01930402059074	2.86147591438449
H	1.70550212793817	1.65721368051403	1.80502991896316
H	2.65943665837987	3.14363398004705	1.71351624461852
C	2.35068804219605	0.94522914454125	4.37379205422691
H	1.51712047525702	1.44222829539532	4.87734093187020
H	3.01379338459153	0.53587054672476	5.14049014645280
H	1.94227645263344	0.10508463931629	3.80272606328383
C	7.17507209013731	5.91679082760972	-0.82791466414699
H	6.42249660961804	6.48653259975376	-0.28016725179266
H	6.68218904858558	5.35578502081845	-1.62142415103566
H	7.87502675852734	6.61467755032890	-1.29334074413410
H	15.12169893491180	4.54282152430825	1.28018922045544
H	15.42456756082400	4.75140221339290	-0.30999203545572
H	11.03241512602460	2.33423991054505	-0.50947052626966
H	10.99881162507320	3.52109108376459	-1.62830713388203

Table S8 - Bond lengths for the HIB molecules of the $[PdCl_2(HIB)_2]$ crystal structure, the DFT optimized structures and those found for 188 ibuprofen/ibuprofenate entries on CSD.

Atoms	Mean bond lengths (Å) found on CSD (ibu/ibu$^-$)	Bond lengths (Å) for HIB $[PdCl_2(HIB)_2]$ crystal structure *	Bond lengths (Å) for HIB $[PdCl_2(HIB)_2]$ DFT optimized structure	Bond lengths (Å) for HIB $[PtCl_2(HIB)_2]$ DFT optimized structure
C3-C4	1.383(2)	1.390(6)/1.384(6)	1.3921/1.3922	1.3913/1.3917
C4-C5	1.387(2)	1.392(6)/1.386(6)	1.3848/1.3834	1.3852/1.3852
C5-C8	1.387(2)	1.370(6)/1.379(7)	1.3917/1.3929	1.3932/1.3924
C7-C8	1.385(2)	1.368(6)/1.377(6)	1.3926/1.3910	1.3922/1.3933
C6-C7	1.382(2)	1.356(7)/1.395(6)	1.3867/1.3873	1.3871/1.3885
C8-C9	1.514(3)	1.52(2) [1.533(7)]/ 1.514(7)	1.5019/1.5005	1.5035/1.5032
C3-C6	1.384(2)	1.383(6)/ 1.385(6)	1.3903/1.3893	1.3923/1.3911
C2-C3	1.519(3)	1.525(6)/ 1.514(5)	1.5203/1.5087	1.5178/1.5162
C1-C2	1.521(2)	1.539(6)/ 1.525(5)	1.5161/1.5173	1.5144/1.5159
C2-C13	1.520(3)	1.507(7)/ 1.540(5)	1.5224/1.5334	1.5248/1.5302
C1-O1	1.257(5)	1.226(5)/ 1.224(4)	1.2149/1.2130	1.2139/1.2159
C9-C10	1.513(4)	1.61(2) [1.562(9)]/ 1.536(8)	1.5369/1.5366	1.5351/1.5374
C10-C12	1.507(7)	1.43(3) [1.47(1)]/ 1.527(9)	1.5214/1.5213	1.5209/1.5244
C10-C11	1.510(5)	1.49(3) [1.50(1)]/ 1.47(1)	1.5223/1.5228	1.5217/1.5219
C1-N2	-	1.338(5)/1.355(4)	1.3672/1.3772	1.3723/1.3654
N2-N1	-	1.408(4)/1.425(4)	1.4064/1.4054	1.4067/1.4081

*the values in braces corresponds to the bond lengths of the disordered groups with lower level of occupation.

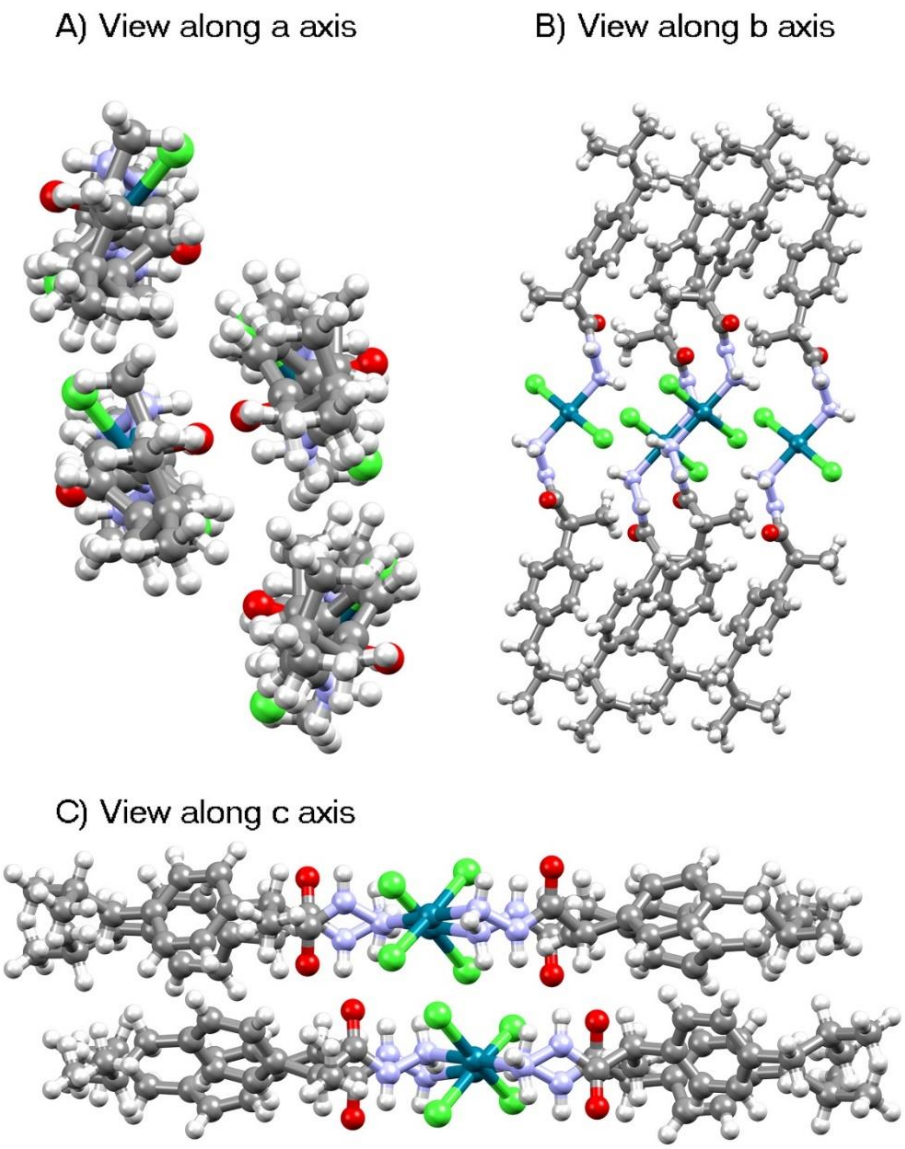

Figure S1. Crystal packing of the complex PdHIB obtained by single crystal X-ray diffraction. The views along axes a, b and c are shown.

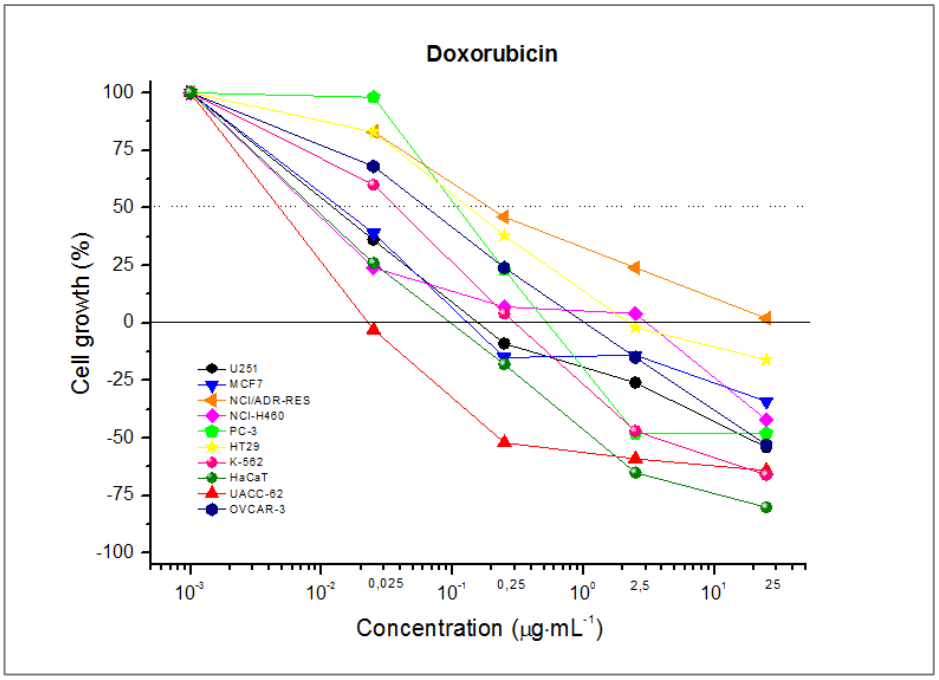

Figure S2. Antiproliferative profile of the positive control doxorubicin.

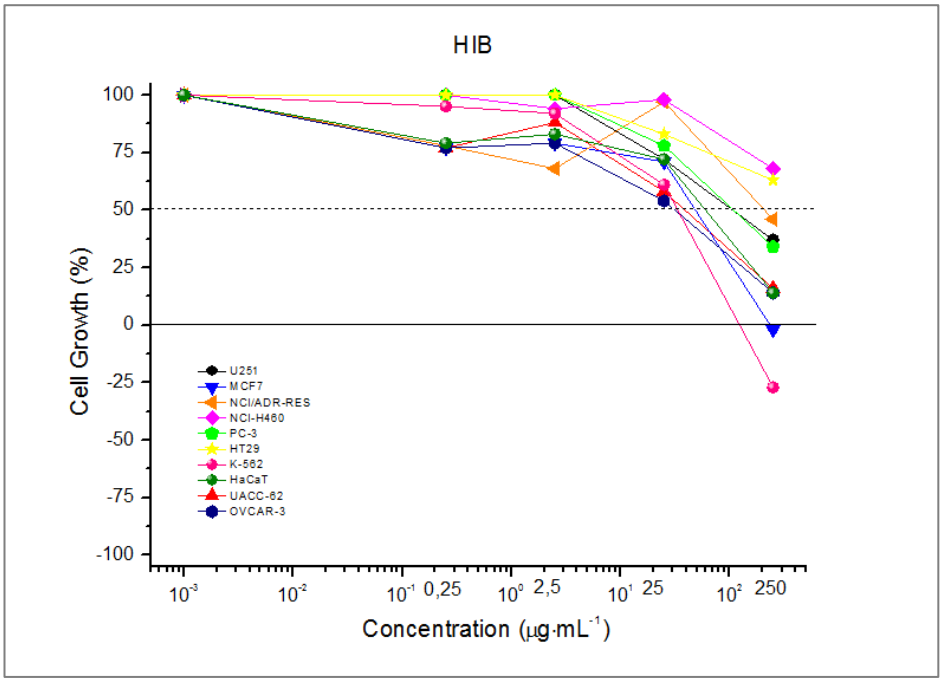

Figure S3. Antiproliferative profile of HIB.

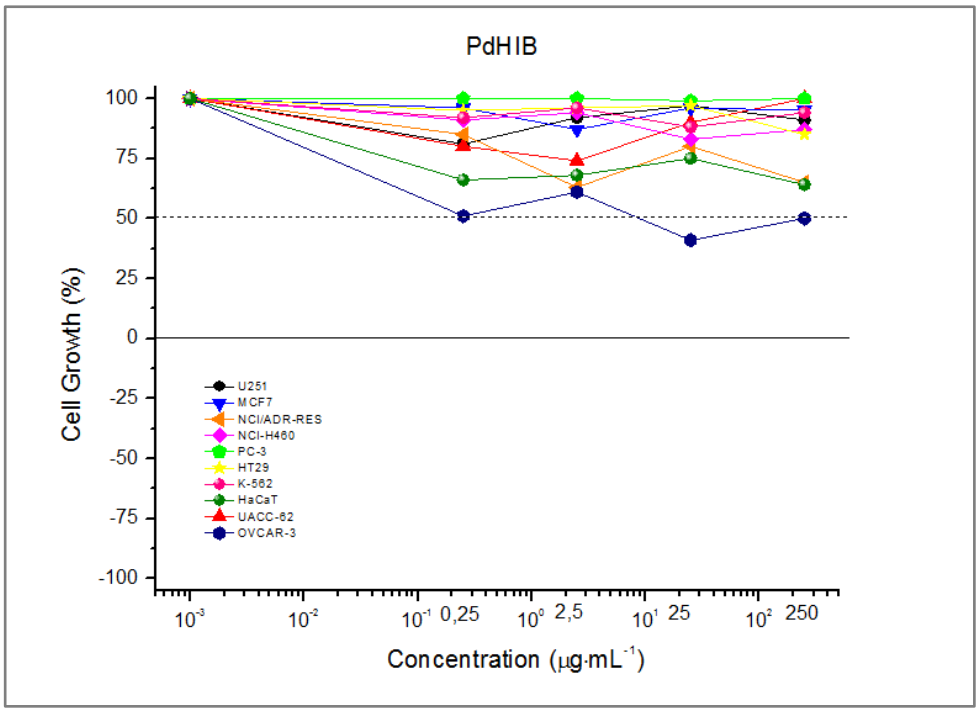

Figure S4. Antiproliferative profile of $[PdCl_2(HIB)_2]$.

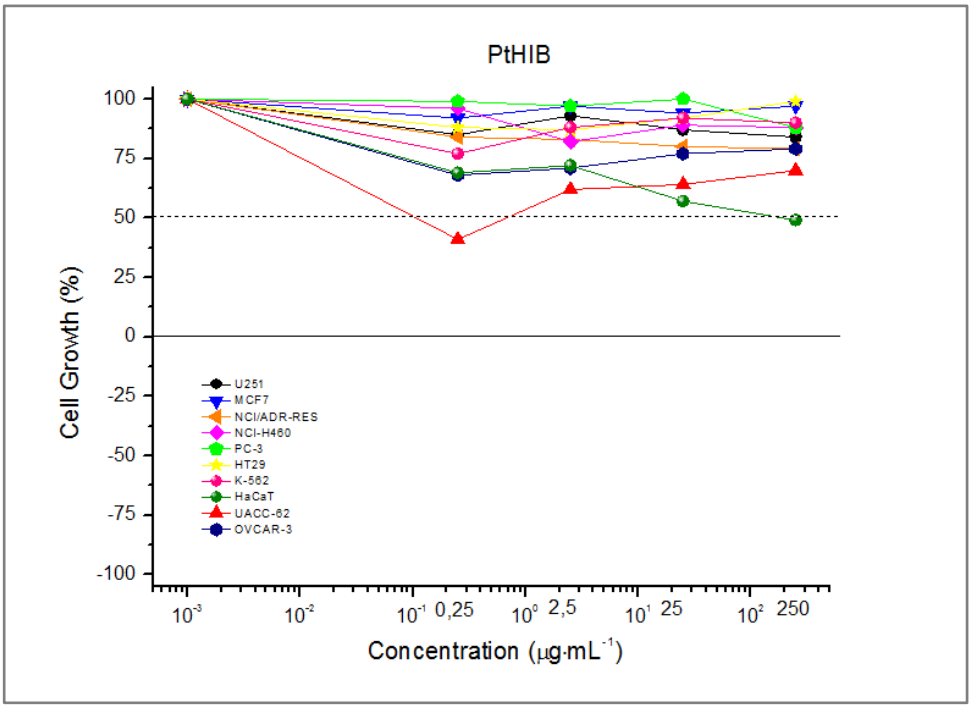

Figure S5. Antiproliferative profile of $[PtCl_2(HIB)_2]$.

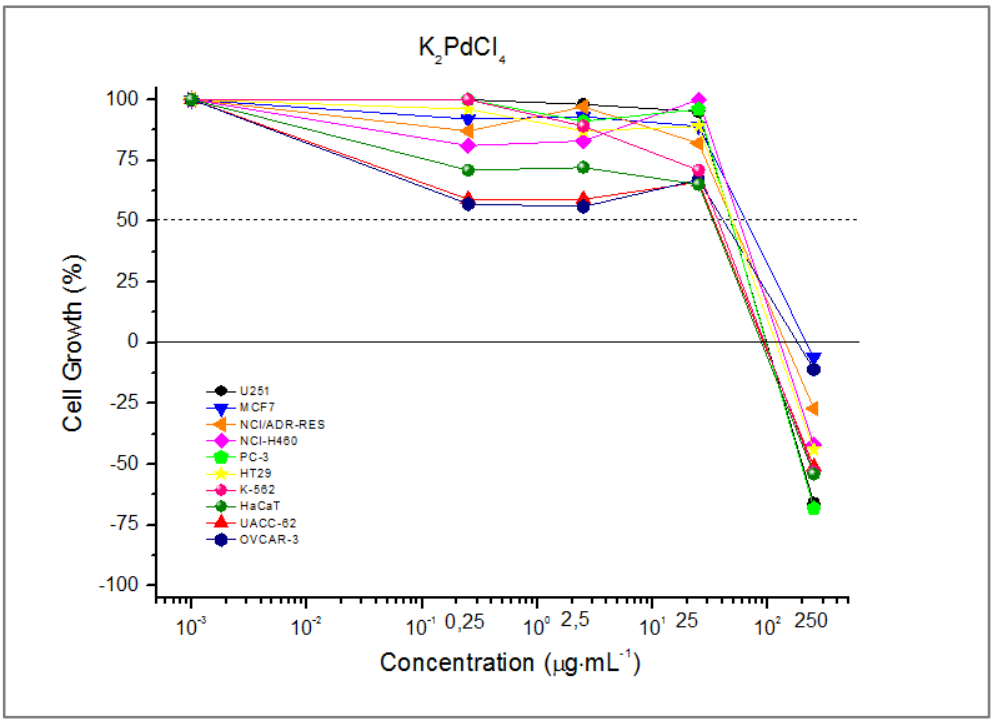

Figure S6. Antiproliferative profile of K_2PdCl_4.

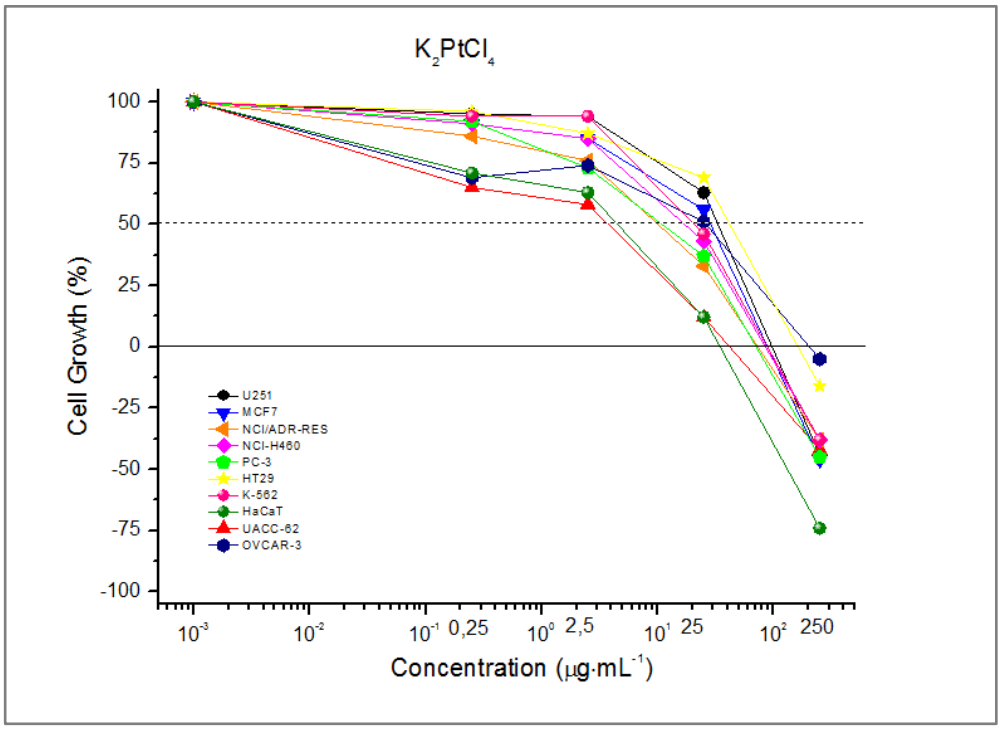

Figure S7. Antiproliferative profile of K_2PdCl_4.